geosciences

MDPI

Article

Impacts of Land Use on Soil Erosion: RUSLE Analysis in a Sub-Basin of the Peruvian Amazon (2016–2022)

Moises Ascencio-Sanchez [1,2,*], Cesar Padilla-Castro [1], Christian Riveros-Lizana [1], Rosa María Hermoza-Espezúa [2], Dayan Atalluz-Ganoza [1] and Richard Solórzano-Acosta [3]

[1] Directorate of Supervision and Control of the Agrarian Experimental Stations (Dirección de Supervisión y Monitoreo en las Estaciones Experimentales Agrarias), National Institute of Agrarian Innovation (Instituto Nacional de Innovación Agraria—INIA), Av. Centenario km 4.00, Pucallpa 25002, Peru; cesar.padillacastro@outlook.com (C.P.-C.); 20240310@lamolina.edu.pe (C.R.-L.); atalluzd@gmail.com (D.A.-G.)

[2] Faculty of Forestry, La Molina National Agrarian University (Universidad Nacional Agraria La Molina), Av. La Molina s/n, Lima 15024, Peru; rosamaria@lamolina.edu.pe

[3] Directorate of Supervision and Control of the Agrarian Experimental Stations (Dirección de Supervisión y Monitoreo en las Estaciones Experimentales Agrarias), National Institute of Agrarian Innovation (Instituto Nacional de Innovación Agraria—INIA), Av. La Molina 1981, Lima 15024, Peru; investigacion_labsaf@inia.gob.pe

* Correspondence: mascenciios@gmail.com; Tel.: +51-988-613-274

Abstract: The Peruvian Amazon faces an increasing threat of soil erosion, driven by unsustainable agricultural practices and accelerated deforestation. In Neshuya (Ucayali region), agricultural activity has intensified since 2014, but the effect on soil erosion is unknown. The present study aimed to evaluate the increase in erosion levels, at a sub-basin of the central–eastern Amazon of Peru, in a Geographic Information System (GIS) environment. The revised universal soil loss equation (RUSLE) model was used for assessing the effect of vegetation cover change from 2016 to 2022. In the Neshuya sub-basin (973.4 km^2), the average erosion increased from 3.87 to 4.55 t ha^{-1} year^{-1}, on average. In addition, there is great spatial variability in the values. In addition, 7.65% of the study area (74.52 km^2) exceeds the soil loss tolerance limit (15 t ha^{-1} year^{-1}). The deforestation rate was 17.99 km^2 year^{-1} and by 2022 the forested area reached 237.65 km^2. In conclusion, the transition from forest to farmland was related to the most critical erosion values. Unsustainable soil management practices can be the underlying explanation of changes in soil chemical and physical properties. Also, social dynamic changes and differences in landscape patterns play a role.

Keywords: degraded tropical soils; Amazonian biome; remote sensing; PISCO SENAMHI; MapBiomass Peru

Academic Editor: Fedor Lisetskii

Received: 6 November 2024
Revised: 24 December 2024
Accepted: 28 December 2024
Published: 6 January 2025

Citation: Ascencio-Sanchez, M.; Padilla-Castro, C.; Riveros-Lizana, C.; Hermoza-Espezúa, R.M.; Atalluz-Ganoza, D.; Solórzano-Acosta, R. Impacts of Land Use on Soil Erosion: RUSLE Analysis in a Sub-Basin of the Peruvian Amazon (2016–2022). *Geosciences* **2025**, *15*, 15. https://doi.org/10.3390/geosciences15010015

1. Introduction

Soil is a non-renewable resource essential for the stability of agroecosystems [1]. Naturally, their properties change over time as part of geological processes. However, anthropogenic activities linked to agricultural activities are causing these processes to accelerate. This is known as soil degradation [2]. In addition, the process of removing topsoil faster than its regeneration, is known as erosion. This can be caused by water or wind and implies a reduction in the effective depth. One of the weather variables which influences it the most is precipitation [3,4]. It causes detachment and horizontal transport of particles from the soil surface. This is called water erosion.

Particle loss from topsoil results in diminished (agro)ecosystems' capabilities to provide goods and services for populations that inhabit them, including human groups [5,6]. Since factors which increase erosion were first studied, it is known that bare soil will show the greatest problems. For example, Bakeley (1977) cited by Ei-Swaify [7] warned that in tropical areas of Africa and Asia, soil loss due to erosion increased when the vegetation cover was reduced. Apart from that, land use change can enhance this greater exposure to weather factors. As indicated by Sepeer (1963), cited by Ei-Swaify [7], reports indicated that in Malaysia cassava (*Manihot esculenta*), banana (*Musa* sp.), pineapple (*Ananas* sp.) and oil palm (*Elaeis guineensis*) crops were associated with serious erosion problems. Meanwhile, in the Amazon biome of Brazil, erosion has intensified due to the deforestation and establishment of crops [8,9]. In this same area, Alyson-Bueno [10] determined a soil erosion average value of 386,422 t ha^{-1} year^{-1} in a highly deforested basin, while Lense et al. [8] reported values from 1.5 to 62.85 t ha^{-1} year^{-1}. In the Peruvian Amazon, where forests' loss and poor soil management has also caused significant problems of erosion [11], Lense et al. [12] calculated erosion rates of 10 t ha^{-1} year^{-1}.

In this study, we focused on the Neshuya area, Ucayali region, where an average erosion of 3.9 t ha^{-1} year^{-1} was estimated by Aybar et al. [13]. The Neshuya sub-basin is found in the Inter-tropical Convergence Zone (ITZC) and it is affected by the interaction of trade winds and the South American Low Level Jet (SALLJ). This creates conditions of intense and persistent rainfall [14,15]. Also, the Andes mountain range, located in Neshuya's western border act as a barrier which modify winds, humidity and precipitation [14]. Neshuya has been experiencing changes in its land cover since 1987 [16–18]. In the last decade, forest cover decreased by more than 50% due to illegal logging followed by migratory agriculture, intensive farming and oil palm plantations [19,20]. These processes of land use change keep affecting the Neshuya sub-basin, so it is necessary to know what effect they have on the erosion levels. Measuring soil loss directly, under field conditions, is costly in terms of time and money, so large-scale evaluations would be unrealistic. That is why the use of indirect measurement methods is presented as an alternative to this problem. In this sense, the application of models fed with more accessible data would increase the feasibility of this type of study. In this research, we will focus on one of the models which calculates soil loss (t ha^{-1} year^{-1}): the revised general soil erosion equation (RUSLE). It will be carried out by estimating each of its parameters, for the Neshuya sub-basin, Ucayali region.

The Universal Soil Loss Equation (USLE), developed by Wischmeier and Smith [21] and its revised version RUSLE [22], are widely used for the calculation of sheet erosion. Models such as RUSLE have been used in various studies in tropical areas and Amazonian basins [8,10,23–25]. They are inexpensive and suitable for inaccessible zones where field data are scarce [12,26]. In RUSLE, erosion is determined by the following factors: climate, vegetation cover type, soil type, topography and human activities [4]. The effect of climate is quantified by the erosivity of rainfall (factor R); the effect of soil type, by soil erodibility (factor K) and slope characteristics (factor LS); the effect of cover type, by vegetation cover (factor C) and finally, the effect of anthropogenic activity, by conservation practices (factor P). The interaction of these factors explains the dynamics of erosion and is crucial for water and soil conservation [7]. The R factor (erosivity) is one of the most important within the RUSLE equation since precipitation is the driving force of erosion. This factor is directly related to the disintegration of soil aggregates and runoff [27]. Some authors mention that between 40% to 90% of eroded soil is due to the effect of precipitation [28–30]. In spite of this, land use type and soil management practices play an important role in deterring the erosive effect of rainfall [31]. The numerical value of the R factor expresses the capacity of the rain to erode the soil [22]. It is defined as the product of the kinetic energy of the

storm and the maximum intensity over 30 min (EI30) [32]. When the study area does not have enough information to determine the value of EI30, alternative equations are applied [25,33]. Data series of more than 20 years of precipitation information are suggested for the calculation of the R factor, because long series allow for the capturing of climate variability and extreme events. This improves the accuracy of the model and helps identify trends [29,34]. Soil erodibility (K factor) is conceptualized as the ease with which soil particles are detached by the effect of rainfall. Fundamentally, it represents the loss of soil per unit of applied external force or energy [22]. Particle size distribution (sand, silt and clay particles) is crucial because it affects infiltration and erosion resistance. On the other hand, organic carbon (percentage of soil organic matter) influences soil cohesion, structure and water retention [35,36]. Soils with high sand content tend to be more friable and less structured, thus becoming more susceptible to erosion [35]. Silt influences cohesion and structure [37]. Higher clay contents can reduce infiltration and increase runoff [38]. Loss of soil carbon due to anthropogenic activities is one of the main causes of soil degradation in the study region [39]. The slope length factor (L) is the distance from where the overland flow originates, to a point of concentration, or a point where the slope gradient decreases and deposition begins. The slope steepness factor (S) defines the influence of the slope gradient on erosion [22]. Both of these two factors are considered to work in combination. The slope length factor (L) is dimensionless, and is defined as the quotient between the annual erosion rate of a plot with a given slope length and the erosion rate of that plot with a standard slope length of 22.13 m [21]. The physiography of the Neshuya sub-basin is hilly and inclined to the east. It has undulating terraces to the west, which become flatter towards the north [40]. The parameter C represents the effects of land cover type [33]. It is defined as a dimensionless number between zero and one, representing the ratio of soil loss from land, under certain vegetation cover conditions to soil loss in bare soil [21,41]. The C factor is very sensitive to changes in soil cover and rainfall dynamics [42]. Vegetation cover is the protection and cushioning element against the erosive force of rain, decreasing the force of the impact of raindrops and surface runoff (Dourojeanni (1967) cited by Fournier [43]; González del Tánago (1991) cited by Aybar et al.) [13]. The conservation practices factor (P) reflects the effect of supporting practices in reducing the amount and speed of water runoff in order to decrease erosion [21]. These authors established that, when no measures are taken to prevent soil loss, like tillage towards the slope gradient, a value of 1 is assigned. The most common support practices are terrace cultivation, strip cultivation and contour cultivation. In the study area, land use practices have been inadequate related to slash-and-burn agriculture, expansion of monocultures and inadequate forest management [39]. Owing to the fact that there is no specific information on the effect of land use changes in the Neshuya sub-basin, Ucayali, the objective of this study was to determine the increase in erosion levels and their spatial distribution, as a consequence of the decrease in natural forest cover and the increase in agricultural area.

We hypothesized that, in the Neshuya sub-basin, water erosion calculated with the RUSLE model increased considerably in 2022, compared to the 2016 base scenario. This is due to the loss of forest cover (ha) and the change in land use oriented towards agricultural activities (ha). The introduction of various cultivated species caused an alteration in the exposure of the soil to precipitation (mm), which modified its properties (physical and chemical) and consequently, contributed to the increase in erosion levels (t ha^{-1} $year^{-1}$). This research applies the RUSLE hydrological model to determine erosion in a Geographic Information System (GIS) environment, and the factors that determine the model were obtained from properly handled satellite information and soil sampling, for the years 2016 and 2022 in the Neshuya sub-basin, Ucayali region, Peru.

2. Materials and Methods

2.1. Area of Study

The research was carried out in the Neshuya River sub-basin located in the district with the same name, within the province of Padre Abad, west of the Ucayali region, Peru. Neshuya River has an extension of 68.9 km and it is a second-order tributary of the Ucayali river. It first joined the Aguaytia river, located in the middle part of the Aguaytia basin. Subsequently, it joins the Ucayali river, contributing with 400 million tons of sediments per year, to the Amazon river [44–46]. The Neshuya sub-basin has an area of 973.4 km^2 of (8°23′20.42″ to 8°52′23.63″ S and 74°51′28.91″ to 75°10′7.29″ W) (Figure 1). The land use types include the following: 55% forest, 25% agriculture, 14% secondary forest and 6% oil palm [18]. The climate in the study area has an annual precipitation of 1800 mm year^{-1}, with a dry season between the months of May and October. The wet season takes place between the months of November and April [47]. The area has a maximum temperature of 30.9 °C, minimum temperature of 19.6 °C, average relative humidity of 77% and annual evapotranspiration of 1200 mm [48]. According to the WRB-FAO soil classification, in the study area, the majority of soils belong to the Acrisols and Cambisols categories. To a lesser extent Ferrasols, Fluvisols and Nitisols are also found [49]. The physiography is mainly made up of moderately inclined and steeply inclined slopes.

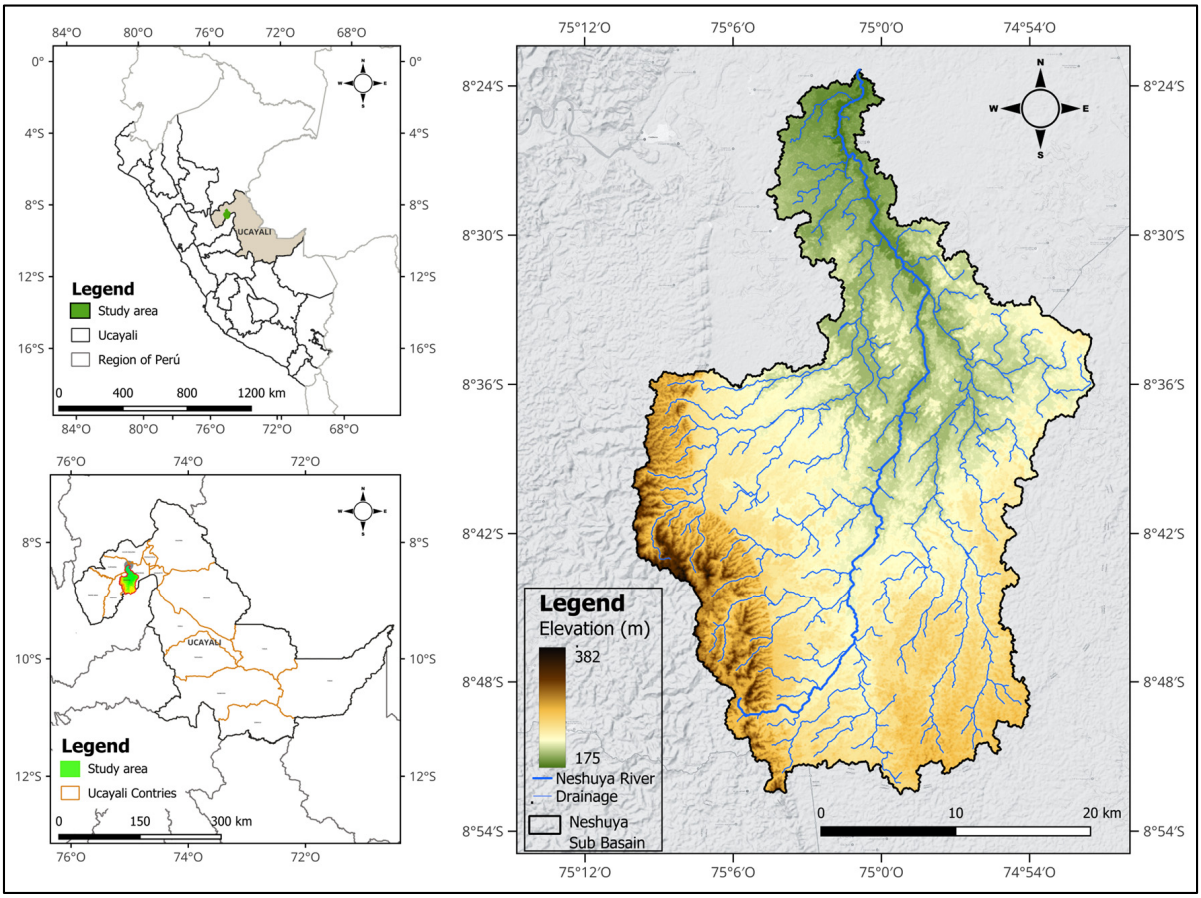

Figure 1. Location of the study area, showing the variability in elevation (m.a.s.l.). Images produced with QGIS software, Version 3.34.6-Prizren http://www.qgis.org/ [50,51] and the SAGA-GIS plugin http://saga-gis.org/ [51].

2.2. Soil Loss Calculation

To determine water erosion, the RUSLE model was applied [22], which is expressed in the following Equation (1):

$$A = R \times K \times L \times S \times C \times P \quad (1)$$

where

A: Soil loss (t ha^{-1} year^{-1})
R: Rainfall erosivity factor (MJ mm ha^{-1} h^{-1} year^{-1})
K: Soil erodibility factor (t ha h MJ^{-1} mm^{-1})
L: Slope length factor (dimensionless)
S: Slope factor (dimensionless)
C: Land cover factor (dimensionless)
P: Conservation practices factor (dimensionless)

2.3. Calculation of RUSLE's Factors

2.3.1. Erosivity Factor (R)

In first place, actual observed precipitation data were obtained from the SENAMHI climate database (Supplementary Materials—S1), for the period 1981–2016 from the following meteorological stations: El Maronal (−8.450000° S; −75.096806° W), Las Palmeras de Ucayali (−8.582500° S; −74.866100° W), San Alejandro (−8.834444° S; −75.216392° W) and Tournavista (−8.927494° S; −74.708817° W). Due to the fact that there were gaps in the data of those stations and they were spatially insufficient, historical precipitation records were obtained from PISCO (Peruvian Interpolated data of the SENAMHI's Climatological and Hydrological Observation) [52]. The downloaded database can be found in Supplementary Materials—S2. The PISCO spatial resolution is 0.1° × 0.1°. This is equivalent to 10 km × 10 km. This resolution mixes weather data from the meteorological stations, satellite data from Climate Hazards Group Infared Precipitation (CHIRP) and radar data [13,52]. PISCO data were generated using the "Residual Ordinary Kriging" (ROK) method. It involves the creation and adjustment of a semivariogram which models the residuals' spatial variability. This technique is suitable for detailed estimations of precipitation and hydrological modelling [52]. According to the criteria of Aybar et al. [52], for our study area, PISCO data are a good representation of the original data. Moreover, Aybar et al. [13], highlights an acceptable correlation coefficient value of 0.75, for this area.

After that, the accuracy of interpolated data at local level was assessed by comparing PISCO data and SENAMHI weather stations' data. The indicators were the following: number of data points for the same period, historical series, calculating a correlation coefficient (r), a determination coefficient (r^2) and the root mean square error (RMSE) [25,53]. The statistical analysis can be found in Supplementary Materials—S3.

The areas without precipitation information were completed with PISCO data; therefore, 42 fictitious stations were generated, obtaining precipitation information for the entire study area for the period 1981 to 2019. At each station, the average monthly and annual precipitation for 38 years were calculated. With these data, the Fournier Index was calculated to characterize the aggressiveness of the rain. Formula (2) was used for each generated station, according to the methodology of Arnoldus [32]. This is suitable for places where it is difficult to find data [27].

$$IFM = \sum_{i=1}^{12} \frac{Pi^2}{P} \quad (2)$$

IFM: Modified Fournier Index
Pi: Monthly precipitation in mm

P: Annual precipitation in mm

After making sure that the value was good enough to interpolate precipitation data from PISCO [54,55] in the QGIS software, the "SAGA Next Gen" plugin was used as well as the "Ordinary Kriging" tool to create isohyets for the average monthly precipitation and the annual average. Subsequently, using the QGIS raster calculator, the equation proposed by Wischmeier and Smith [21] and revised by Arnoldus [32] was used to calculate the R factor (Equation (3)), for each pixel, for each year of the study.

$$R = \sum_{i=1}^{12} 1.735 \times 10^{(1.5\log_{10}(\frac{P_i^2}{P}) - 0.08188)} \quad (3)$$

where

R: Erosivity factor (MJ mm ha^{-1} h^{-1} year^{-1}),

Pi: Monthly precipitation in mm

P: Annual precipitation in mm

2.3.2. Erodibility Factor (K)

The database of INIA laboratory of water, soil and foliar analyses (LABSAF), located at the Campo Verde experimental station (EEA-Pucallpa), was used to identify 74 soil samples, collected in the study area and its surroundings. These samples were processed between 2023 and 2024. Thirty one points were allocated within the Neshuya sub-basin and 43 points in its surroundings. The physical and chemical parameters can be found in Supplementary Materials—S4. With these data, a descriptive analysis was performed to evaluate the level of homogeneity in the soil samples. After that, for each of the samples, the value of the K factor was calculated by applying Equations (4)–(8) proposed by [56], since the texture and organic matter content are directly related to susceptibility to erosion [21]. The results of the calculations can be found in Supplementary Materials—S5.

$$K_{RUSLE} = 0.1317 \times f_{sand} \times f_{cl-si} \times f_{org} \times f_{hisand} \quad (4)$$

where

K: Soil erodibility factor (t ha h MJ^{-1} mm^{-1})

f $_{sand}$: Sand and silt factor

f $_{cl\text{-}si}$: Silt and clay factor

f $_{org}$: Soil organic carbon factor

f $_{hisand}$: Sand factor

$$f_{sand} = \left(0.2 + 0.3 \times \exp\left[-0.256 \times m_s \times \left(1 - \frac{m_{silt}}{100}\right)\right]\right) \quad (5)$$

where

f_{sand}: Sand factor

m_s: Percentage of sand registered by the laboratory in the topsoil layer

m_{silt}: Percentage of silt registered by the laboratory in the topsoil layer

$$f_{(cl-si)} = \left(\frac{m_{silt}}{m_c - m_{silt}}\right)^{0.3} \quad (6)$$

where

$f_{cl\text{-}si}$: Silt and clay factor

m_{silt}: Percentage of silt registered by the laboratory in the topsoil layer

m_c: Percentage of clay registered by the laboratory in the topsoil layer

$$f_{org} = \left(1 - \frac{0.25 \times orgC}{orgC - \exp[3.72 - 2.94 \times orgC]}\right) \quad (7)$$

where

f_{org}: Soil organic carbon factor

orgC: Soil organic carbon % registered by the laboratory in the topsoil layer

$$f_{hisand} = \left(1 - \frac{0.7 \times \left(1 - \frac{m_s}{100}\right)}{\left(1 - \frac{m_s}{100}\right) + \exp\left[5.51 + 22.99 \times 0.7 \times \left(1 - \frac{m_s}{100}\right)\right]}\right) \quad (8)$$

where

f_{hisand}: Sand fraction

m_s: Percentage of sand recorded by the laboratory in the topsoil layer

The values obtained for the K factor were compared with other values in the literature to confirm their validity. The spatial dependence of the K factor was then evaluated in order to perform spatial interpolation according to the method of Lima et al. [35]. For this, an experimental semivariogram of the parameters studied and the K value used was assembled, as recommended by Ahaneku et al. [57], Denton et al. [58,59] and Lima et al. [35]. This can be found in Supplementary Materials—S6. The main parameters evaluated were Nugget (Co), Sill (Co + C) and Range (A). The criterion for classifying spatial dependence (SDE) was the relationship between Nugget and Sill (Co/Co + C). This indicates the degree of correlation between the sample points. If SDE < 25%, the variables have strong spatial dependence; if it is between 25% and 75%, it is moderate; if it is between 75% and 100%, it is weak; finally, if the relationship is greater than 100%, it indicates that the variables have no spatial correlation [35,57]. Based on the statistical and geostatistical analysis, the "Inverse distance weighting" (IDW) method was used to calculate each soil property, for each pixel, in each year of study. Finally, the K factor was calculated in the raster calculator of the QGIS software, applying Equations (4)–(8).

2.3.3. Topographic Factor (LS)

The calculation of the L and S factors required a Digital Elevation Model (DEM). This was obtained from the ALOS-PALSAR satellite with a resolution of 12.5 m × 12.5 m, downloaded from the free data platform "ASF Data Search" of [59]. The HEC-HMS program, version 4.1 [60] was used to perform the "fill" correction of the DEM and eliminate imperfections (depressions and sinkholes). The procedures for calculating the L and S factors for each pixel were carried out in the QGIS software. To calculate the L factor, Equations (9)–(11), proposed by Desment et al. [61], were used. Equation (9) allows for the slope angle to be obtained in sexagesimal degrees. This was applied using the raster calculator of the QGIS software.

$$\beta = \frac{\frac{sin\theta}{0.0896}}{3(sin\theta)^{0.8} + 0.56} \quad (9)$$

where

β: Pixel level slope

θ: Slope angle in sexagesimal degrees

Equation (10) was then applied to obtain the "m" value. Finally, to obtain the L factor values, Equation (11) was used; however, the "A" value had to be previously calculated, which represents the accumulated flow. For this, the "SAGA Next Gen" plugin and the

"Catchment area" tool (flow tracing) were used in the corrected DEM. The value of "*D*" corresponds to the pixel size of the DEM (12 m × 12 m).

$$m = \frac{\beta}{(1+\beta)} \tag{10}$$

where

m: Dimensionless factor

β: Pixel level slope

$$L_{(i,j)} = \frac{\left(A_{(i,j)+D^2}\right)^{m+1} + A_{(i,j)^{m+1}}}{D^{m+2} \times (22.13)^m} \tag{11}$$

where

L: Slope length factor (dimensionless)

A: Accumulated flow

m: Dimensionless factor of Equation (10)

D: Pixel size

For the S factor, Equations (12) and (13) of McCool et al. (1997) cited in Renard et al. [22] were used. This was calculated for each pixel.

$$S = 10.8 * \sin\theta + 0.03, Si : S < 9\% \tag{12}$$

$$S = 16.8 * \sin\theta - 0.5, Si : S \geq 9\% \tag{13}$$

where

S: Slope inclination

θ: Slope angle in sexagesimal degrees

2.3.4. Plant Cover Factor (C)

Data of land cover were obtained from the MapBiomas Peru Collection 2.0 [62]. This group of data used annual mosaics from Landsat 4 to 9 series (1985 to 2022). It combines multiple observations for each pixel, which helps to reduce interference. Image classification is based on the Random Forest method, and the algorithms are available at MapBiomas Peru GitHub [62]. The precision assessment included field validation, sampling of 71,500 pixels and metrics like the mapping precision, pixel assignation mismatch and area. Data of land cover were downloaded from Google Earth Engine (GEE), using an open code given by MapBiomas Peru [62], for the years 2016 and 2022. Data were obtained in raster format, and were imported to QGIS software. Then, the data were transformed into vector format. Use categories were assigned according to the "General legend of land use and cover in the Collection 2.0" [62]. After that, the Factor C value was assigned according to a literature review performed in research works which took place at similar latitudes, at tropical humid locations. Information came from the following studies: West Africa [7], Malaysia [63–65], Indonesia [66–68] and Brazil [10,41,42,69]. In the latter country, studies on the C factor based on permanent field plots are scarce and only performed during short periods of time. Research that gives C values by specific crop type was also reviewed [7,70]. Chosen values considered the frequency of repetition by cover type. In the case of agricultural mosaic, it groups crops such as cassava, maize, banana, papaya and cocoa; therefore, the average value was taken. They can be found in the Section 3 of this factor.

2.3.5. Conservation Practices Factor (P)

The value of the P factor was estimated in the following way. Visits were made to specific points of the sub-basin to evaluate the soil conservation practices applied by the farmers. It was not possible to specifically evaluate each plot since it is economically unviable. The paved roads' data were obtained from the spatial data website of the "Ministry of Transport and Communications of Peru-MTC" [71], then the information was visualized in the QGIS software to validate the presence of them.

Then, values were assigned based on the conservation practice applied to each type of soil cover. In forest areas, no activities are carried out on the soil; therefore, a value of 1 is considered [72]. In agricultural areas, conservation practices were assessed and if these were not applied, a value of 1 was considered; otherwise, lower values were assigned. In the case of pastures, since they are not cultivated, but rather grow naturally after the farmland is abandoned, a value of 1 was assigned. The number of paved roads was evaluated and assessed based on the percentage of representativeness with respect to the sub-basin under study. Bare soil was assigned a value of 1 since it does not present any type of conservation practice.

2.4. Calculation of Erosion and Classification by Levels and Type of Coverage

After determining the factors "R", "K", "LS" and "C", the rasters of each factor were scaled to pixels of 12.5 m × 12.5 m in the QGIS raster calculator. This was because the "LS" factor had the smallest pixel size, so in that way, consistency was achieved. Afterwards, Equation (1) was applied and erosion was calculated for each pixel for the years 2016 and 2022. Considering that the study area is located in a humid tropical zone, a soil loss tolerance limit of 15 t ha^{-1} $year^{-1}$ was established, according to studies carried out by Mannigel et al. [73] and Nunes et al. [38]. Erosion was then classified into erosion levels based on studies carried out in the Brazilian Amazon [8,12]. Finally, considering the vegetation cover type, the area of each erosion level was calculated for palm, pasture, agricultural mosaic, bare soil (including roads, cities and bare soil) and forest (including flooded and non-flooded forest) for the years 2016 and 2022. Also, the deforested area in the study period and the areas that exceed the soil loss tolerance limit of 15 t ha^{-1} $year^{-1}$ were calculated.

3. Results

3.1. R Factor

The significance of the correlation coefficients (p-value) is below 0.05, indicating that all correlations are statistically significant at a confidence level of 95%. The correlation coefficients of the stations "El Maronal, San Alejandro and Tournavista" are very high ($r > 0.95$) (Table 1). This implies the existence of a strong linear relationship between the observed data and those of PISCO. The root mean square error (RMSE) is higher in "Las Palmeras de Ucayali"; however, the quality of the correlation is adequate (Table 1). More details of the statistical procedure, correlation graphs, historical series and error distribution can be found in Supplementary Materials—S7.

The monthly and annual precipitation data generated for the 42 fictitious stations, from 1981 to 2019, can be found in Supplementary Materials—S8. The IFM calculations for each of the 42 fictitious stations can be found in Supplementary Materials—S9. The descriptive statistical summary indicated that all the calculated IFM data exceeded the value of 140 for the study area, standard deviation of 33.6 and coefficient of variability of 17% for the study area. According to Lobo et al. [74], the study area is classified as a zone with high and very high erosive potential (Table 2).

Table 1. Monthly precipitation correlation statistics between weather stations and PISCO SENAMHI.

Weather Station	Correlation Coefficient (r)	Type of Correlation	RMSE	Number of Observations (Months)	Correlation Coefficient Significance (p_Value)
'El Maronal'	0.963	very high	31.88	283	$1.8954 \times 10^{-160} < 0.05$
Las Palmeras de Ucayali	0.766	high	75.58	249	$2.3767 \times 10^{-51} < 0.05$
San Alejandro	0.959	very high	33.824	240	$3.3720 \times 10^{-132} < 0.05$
Tournavista	0.964	very high	33.646	276	$4.7058 \times 10^{-158} < 0.05$

Note: Details of the statistical analyses can be found in Supplementary Materials—S7.

Table 2. Modified Fournier Index (IFM) classification, adapted to Latin America.

IFM	Classification
0–60	very low
60–90	low
90–120	moderate
120–160	high
>160	very high

Source: [74].

The results of the correlation analysis between the IFM and the R factor then indicated a high coefficient of determination, $r^2 = 0.97$ (Figure 2). In this way, we concluded that R factor obtained from Equation (3) is a good estimator of the erosivity within the assessed area.

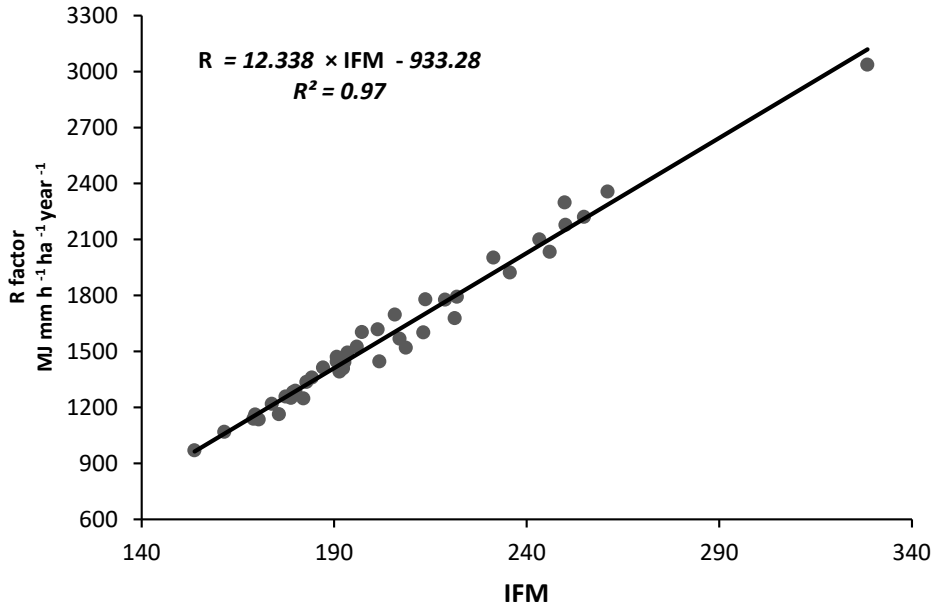

Figure 2. Correlation of the R factor and the Modified Fournier Index (MFI).

The result of the R Factor analysis in the Neshuya sub-basin reveals an average value of 1512.34 MJ mm ha^{-1} h^{-1} $year^{-1}$ and a standard deviation of 279.03, demonstrating that the erosive potential is moderate to high (Supplementary Materials—S10). The results of precipitation and R Factor, for each pixel of the study area, can be seen in Figure 3. It shows the great spatial variability and also that the highest values were greater than 2000 MJ mm ha^{-1} h^{-1} $year^{-1}$. They were found at the southeast of the Neshuya sub-basin because this area had the highest accumulated annual precipitation. Downstream of the study area, the specific values varied from 1100 to 1300 MJ mm ha^{-1} h^{-1} $year^{-1}$.

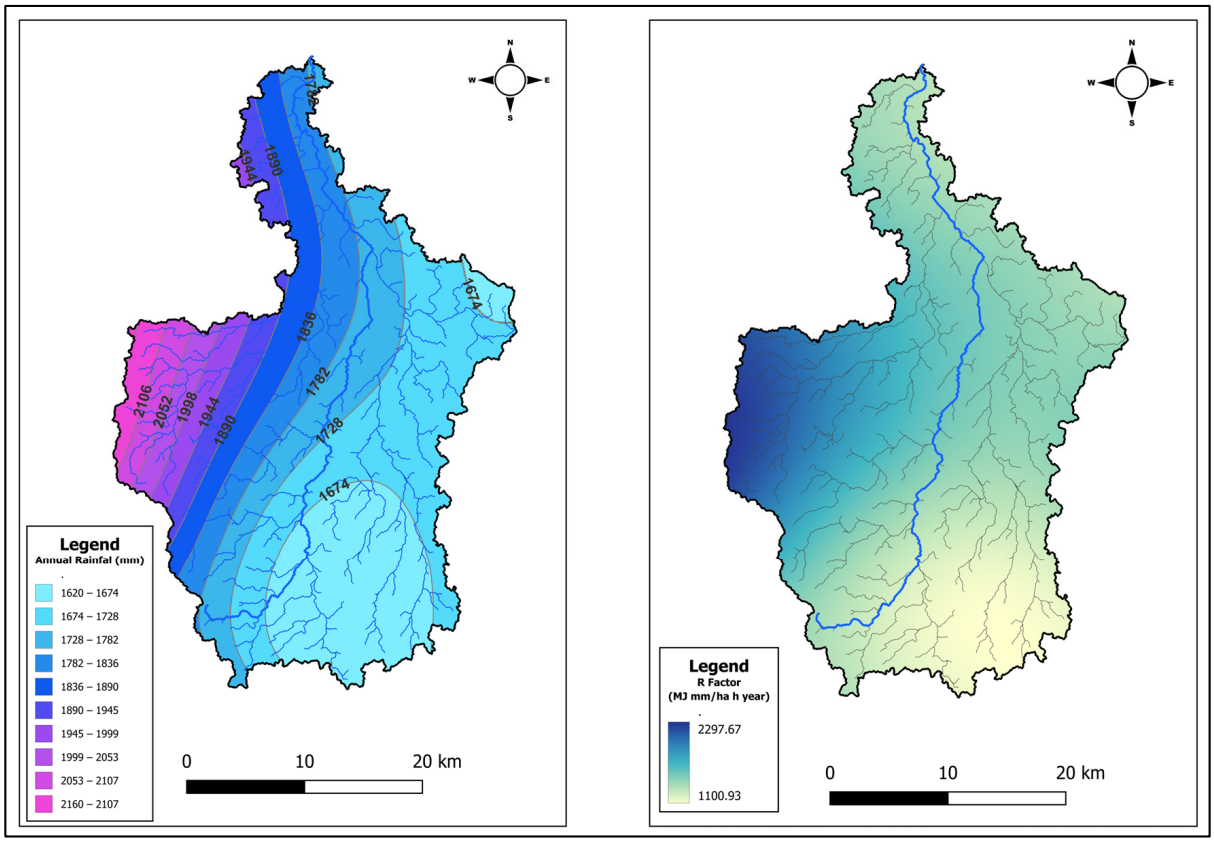

Figure 3. Spatial distribution of the average annual accumulated precipitation, analyzed for the period from 1981 to 2019 (**left**) and the calculated values of the R factor (**right**), of the Neshuya sub-basin, Ucayali region. Images produced with QGIS software, Version 3.34.6-Prizren http://www.qgis.org/ [50]; and Ordinary kriging algorithm performed with SAGA-GIS plugin http://saga-gis.org/ [51].

3.2. K Factor

Soil characterization results indicate that particle size distribution takes wide values. Sand varies from 11.12% to 84.29% and clay varies from 7.10% to 60.38%. In addition, sand was found in greater proportion than clay in most of the samples, while the proportion of silt (7.14 to 52.37%) showed the lowest coefficient of variation among the four particle sizes. Organic matter is low in most of the samples (2.1%) and presents the highest coefficient of variation (60%) finding values from 0.13% to 7.8%. Out of the 74 samples, it was found that loamy textures predominate in the study area (Table 3).

Table 3. Descriptive statistics of the 74 soil samples * and correlation coefficient with K factor value.

Fraction	Average (%)	Min. (%)	Max. (%)	Standard Deviation	CV (%)	K Correlation Coef.
Sand (%)	43.41	11.12	84.29	13.28	31	0.03
Silt (%)	29.75	7.14	52.37	8.46	28	0.46
Clay (%)	26.84	7.1	60.38	10.28	38	−0.42
MO (%)	2.1	0.13	7.8	1.26	60	−0.70

* Number of samples associated with each textural class: clay (6), sandy clay (2), silty clay (2), loamy sand (1), loam (16), sandy clay loam (14), clay loam (20), sandy loam (12), silty loam (1).

The results of the calculation of the K factor for each of the 74 samples can be found in Supplementary Materials—S5. The values range from 0.0122 to 0.0239 t ha h MJ^{-1} mm^{-1}. Table 4 shows the results of the bibliographic review of erodibility in tropical soils such as Cambisols and Argisols, which are the ones that dominate the study area. However, they are not strictly equal since there are differences in the mineralogical composition and soil aggregates, among others. The values presented correspond to field work (Table 3), while bibliographic data allow us to validate the applied methodology (Table 4). The values found in our work fit with the values found by the cited authors (Table 4)

Table 4. Soil erodibility.

Textural Class	K Factor t ha h MJ^{-1} mm^{-1}	Bibliographic Source
Loamy sand	0.008	Angulo [75]
Sandy loam	0.034	Tovara et al. 1985 cited by Silva et al. [37]
Sandy clay loam	0.007; 0.026	Angulo [75]; Martins et al. [76]
Sandy clay	0.0004; 0.0115; 0.034	Angulo [75]; Silva et al. [37]
Clay	0.002; 0.0045; 0.025	Marques et al. [77]; Mondargo 1978 cited by [37]; Silva et al. [37]

The results of the spatial dependence analysis of the K factor indicated the following. The Nugget (Co) represents the variability at very short scales. High values of sand, silt and clay indicate a considerable variability at very small scales or inconsistency in the measurement (Table 5). The Sill values (Co + C) show a low increase indicating a weak spatial structure. The OM and the K factor suggest low spatial variance (Table 5). The Range (A) range indicates the correlation at long distances. The values found are high, suggesting that at large distances, there are correlations (Table 5). The RMSE (root mean square error) of sand, silt and clay indicate that the proposed models fit poorly, except for OM which shows a better fit (Table 5). The low R^2 values indicate that the models do not explain the variance of the parameters. The SDE for sand and silt show that there is no spatial correlation. For clay and OM, it is not significant. which indicates that there is little or no spatial relationship [58,78] (Table 5).

Table 5. Parameters of the semivariograms for the variables sand, silt, clay, OM and K factor.

Parameter	Model	Nugget Co	Sill Co + C	A (Range)	RMSE	R^2	SDE (%) Co/Co + C
Sand	Sph	209.84	164.347	13,931.168	4,976,180.515	0.007	128%
Silt	Gau	93.624	70.28	5742.932	1,021,137.486	0.005	133%
Clay	Linear	87.686	100.751	18,610.93	2,752,316.58	0.008	87%
OM	Sph	1.224	1.645	10,102.697	923.055	0.002	74%
K Factor	Gau	0	0	0	0	−0.038	---

Although the geostatistical analysis showed a very low correlation between the sampling points, a map was constructed with the interpolated results of the K factor applying the IDW method (Figure 4).

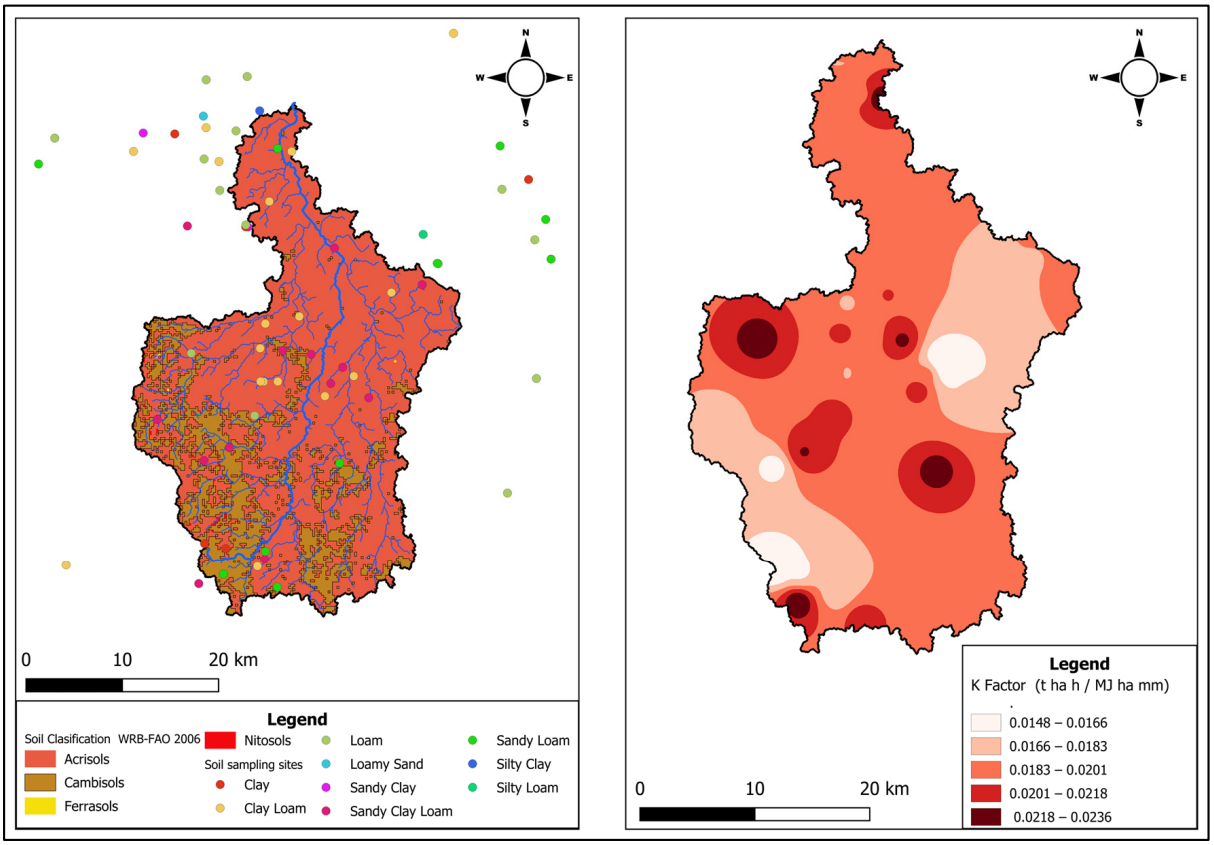

Figure 4. Spatial distribution of sampling points and soil types obtained from SoilGrids (version 2.0 https://soilgrids.org/) [49] (**left**) and calculated values of the K factor (**right**), for the Neshuya sub-basin, Ucayali region. Images produced with QGIS software (version 3.34.6-Prizren http://www.qgis.org/) [50]; and QGIS IDW algorithm.

3.3. LS Factor

The results of the LS factor indicate that, in the Neshuya sub-basin, the topography is steeper towards the west and flatter towards the northeast. It can be seen that the relief is hilly with slopes from 3% to 14% (Figure 5). This indicates soils that are more prone to erosion when uncovered. Areas with values from 2 to 4 for this factor, which are not grouped together as in the western area, were also observed (Figure 5). Their presence indicates soils that are prone to erosion when uncovered too (Table 6).

Table 6. Range of LS factor values in each slope range.

Slope (%)	LS Factor
0–3.3	0–0.5
3.3–6.5	0.5–1
6.5–9	1–1.5
9–11	1.5–2
11–14	2–2.5
14–21	2.5–4
21–35	4–6.25

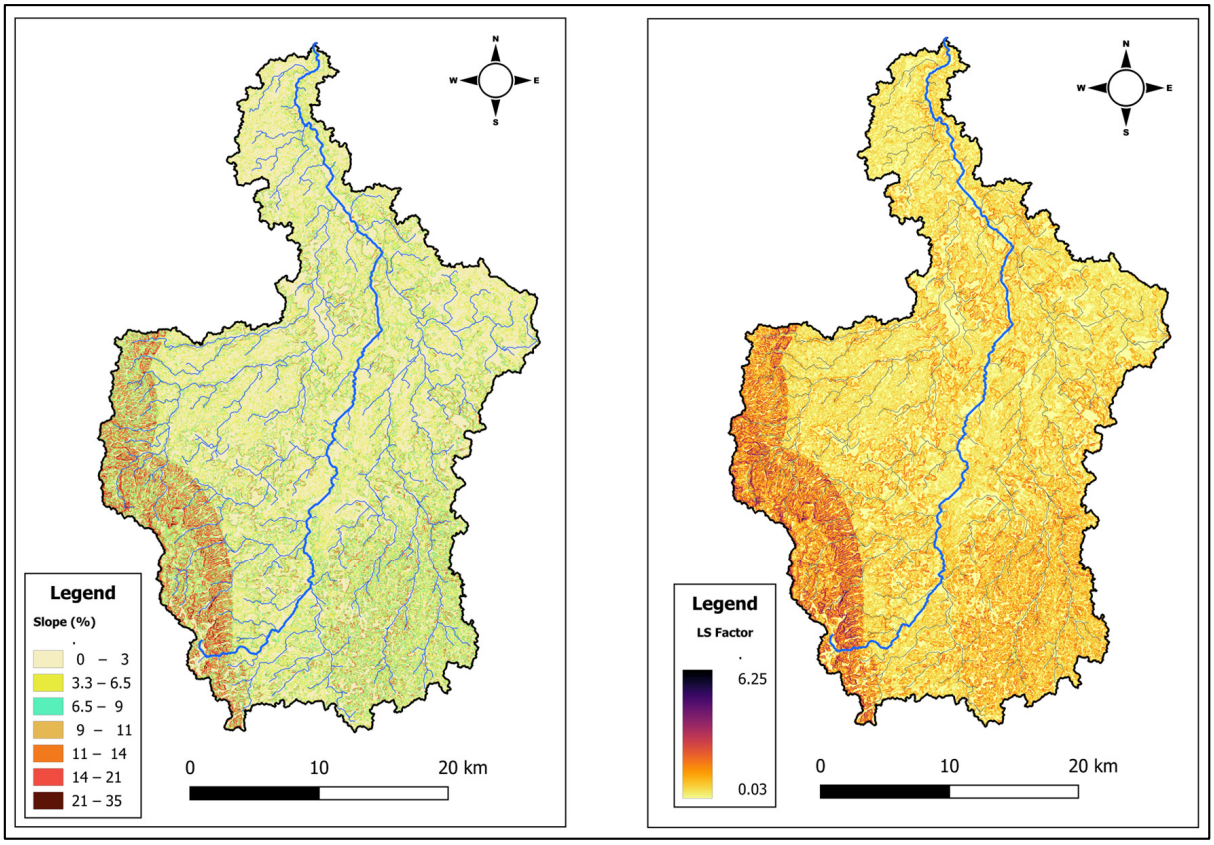

Figure 5. Spatial distribution of the slope (**left**) and LS factor (**right**) values found for the Neshuya sub-basin, Ucayali region. Images produced with QGIS software (version 3.34.6-Prizren http://www.qgis.org/) [50].

3.4. Factor C and Change of Coverage

The results of the literature review of factor C can be found in Table 7.

Table 7. Soil cover factor C.

Ground Cover	Factor C	Bibliographic Source
Forest	0.001	Alyson Bueno [10]; ICC et al. [70]; Kamaludin et al. [64]; Naharuddin [67,68]; Oliveira et al. [41]; Putra et al. [79]; Rosee (1997) cited by Ei-Swaify [7].
Flooded forest	0.001	Kamaludin et al. [64]; Rosee (1997) cited by Ei-Swaify [7];
Oil Palm	0.3	Kamaludin et al. [64]; Ramadhan et al. [66]; Rosee (1997) cited by Ei-Swaify [7]
Pasture	0.1	Almagro et al. [42]; Alyson Bueno [10]; ICC et al. [70]; Naharuddin [67,68]; Rosee (1997) cited by Ei-Swaify [7].
Agricultural mosaic	0.4	Rosee (1997) cited by Ei-Swaify [7]; DID [65]; Martins et al. [24]; Naharuddin [67,68];
Bare ground	1	Almagro et al. [42]; Kamaludin et al. [64]; Naharuddin [67,68]; Rose (1997) cited by Ei-Swaify [7]
Roads and cities	1	Almagro et al. [42]; Ramadhan et al. [66]; Rose (1997) cited by Ei-Swaify [7]; Kamaludin et al. [64]; Naharuddin [67,68]

The land cover type data had an overall mapping accuracy of 87.4% (quite high), an assigned discordance value of 2.5% indicating few pixel assignment errors, an area discordance of 10% which is acceptable for the Amazon and a confidence level of 95% [62]. Therefore, they are suitable for coverage analysis in the Amazon region [80,81].

Eight types of land use categories were found (Figure 6): forest and flooding forest with multi-layered vertical structure, that offer great protection to the soil; agricultural mosaic, which groups traditional crops of the study area; oil palm (*Elaeis guineensis*) which is an industrial introduced crop; and pasture, which groups several species that grow naturally after the abandonment of cultivated areas. Also, bare soil is considered an area which does not show vegetation or other type of protection for most of the year. Finally, roads and cities are anthropic areas where people settle periodically or permanently according to their agricultural activities. Due to the socioeconomic characteristics of the study area, they are mainly bare soil.

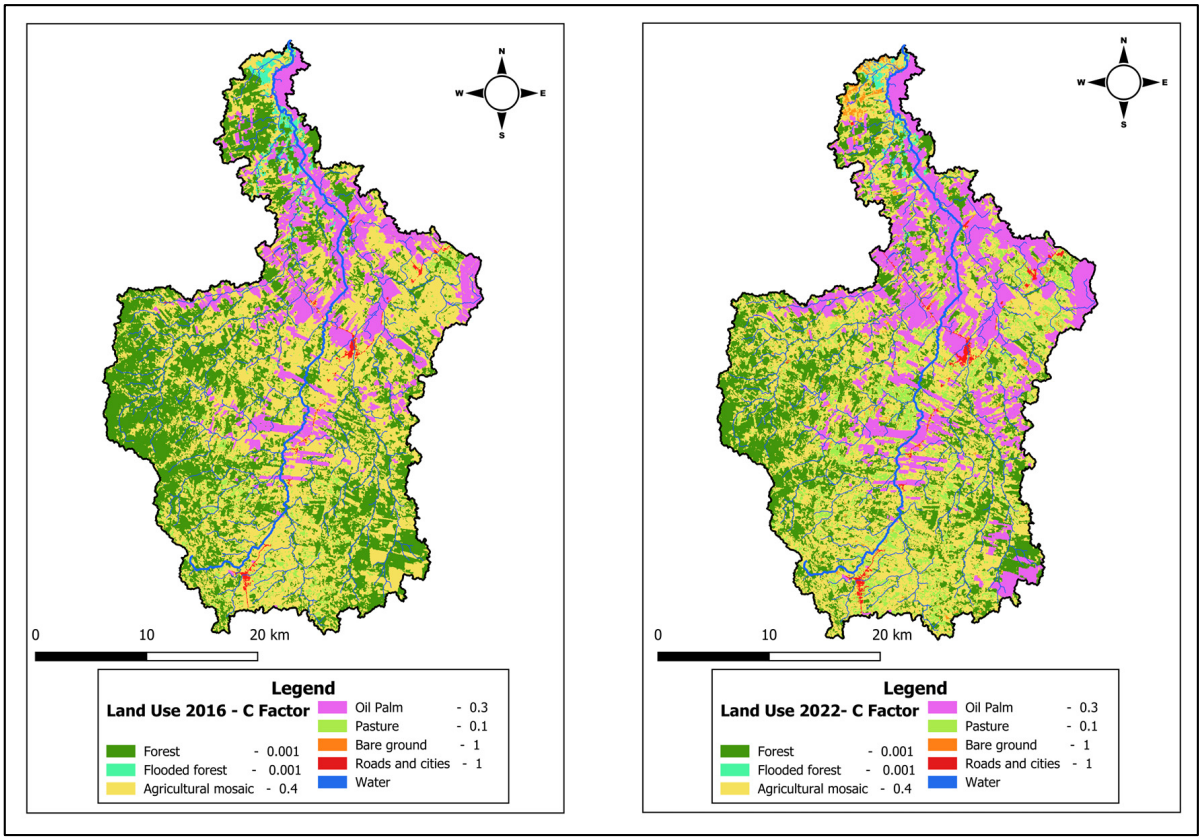

Figure 6. Spatial distribution of values found for the C factor for the years 2016 (**left**) and 2022 (**right**), indicating the land use type, in the Neshuya sub-basin, Ucayali region. Images produced with QGIS software (version 3.34.6-Prizren http://www.qgis.org/) [50] based on data Proyecto MapBiomas Peru (2023) available at https://peru.mapbiomas.org/herramientas/ (accessed on 1 January 2024)).

It was found that deforestation, defined as the change of forest (both non flooded and flooded) to another land use type except water, was 107.96 km^2. This represents a loss rate of 17.99 km^2 year^{-1} and corresponds to the cover that showed the greatest change. In addition, the agricultural mosaic category decreased by 25.43 km^2. On the other hand, the main covers which increased were oil palm (64.69 km^2) and pasture (55.09 km^2). Furthermore, the agricultural mosaic which in 2022 occupied 96.19 km^2, used to be forest in 2016. Also, oil palm occupied 56.72 km^2 in 2022 which used to belong to agricultural mosaic category in 2016. In general, 27.4% of the sub-basin area changed the type of coverage in 2022 compared to 2016 (Table 8).

Table 8. Area by land use type in 2016 and 2022.

Type of Coverage	2016 Area (km^2)	2022 Area (km^2)	Variation Area (km^2)
Forest	340.41	237.65	−102.76
Flooded forest	11.23	6.03	−5.2
Pasture	23.62	78.71	+55.09
Agricultural mosaic	447.78	422.35	−25.43
Roads and Cities	4.68	6.49	+1.81
Bare ground	0.31	11.69	+11.38
Water	1.34	1.75	+0.41
Palm	143.65	208.34	+64.69
Total area	972.99	972.99	266.36 *

* Sum of absolute values for all the variation in areas.

3.5. P Factor

It was observed that soil conservation practices are not put into practice in the Neshuya sub-basin. Figure 7 shows that agricultural crops are established in previously deforested areas. These crops do not have any type of design to avoid soil loss due to rainfall. No agroforestry practices were observed either. On the other hand, pastures grow after the soil becomes unproductive and is abandoned. No type of pasture management or practice is carried out, and overgrazing was observed in some areas, which further degrades the soil. In the case of intensive crops such as oil palm, soil vegetation is continually removed to avoid competition for nutrients, leaving the soil almost bare.

Figure 7. Typical landscape and land use of the Neshuya sub-basin, showing that conservation practices are not applied to the different types of vegetation cover. (**A**) Deforested area for the establishment of shifting agriculture, with cocoa (*Theobroma cacao*) crops in the direction of the slope, without soil conservation practices or agroforestry systems; behind the cocoa crops, intact tropical forest is observed. (**B**) Pasture that emerges naturally on abandoned land by agriculture due to low fertility. No conservation practices are used as it is not economically viable. (**C**) Oil palm plantations

(*Elaeis guineensis*) show little protection offered by the palm leaves. Soil vegetation is continually removed mechanically or with herbicides to reduce competition for nutrients, leaving the soil with very little protection. (**D**) Soil left uncovered for long periods of time in areas where the vegetation cover was removed to carry out various activities such as establishing temporary camps, new crops or is abandoned due to its low fertility.

Regarding the roads, it was calculated that there are 0.435 km^2 of paved roads in the Neshuya sub-basin, which represents 0.04% of the study area. Figure 8 shows that only the main road is paved; the secondary roads in the city lack this protection and are completely uncovered, leaving the soil exposed.

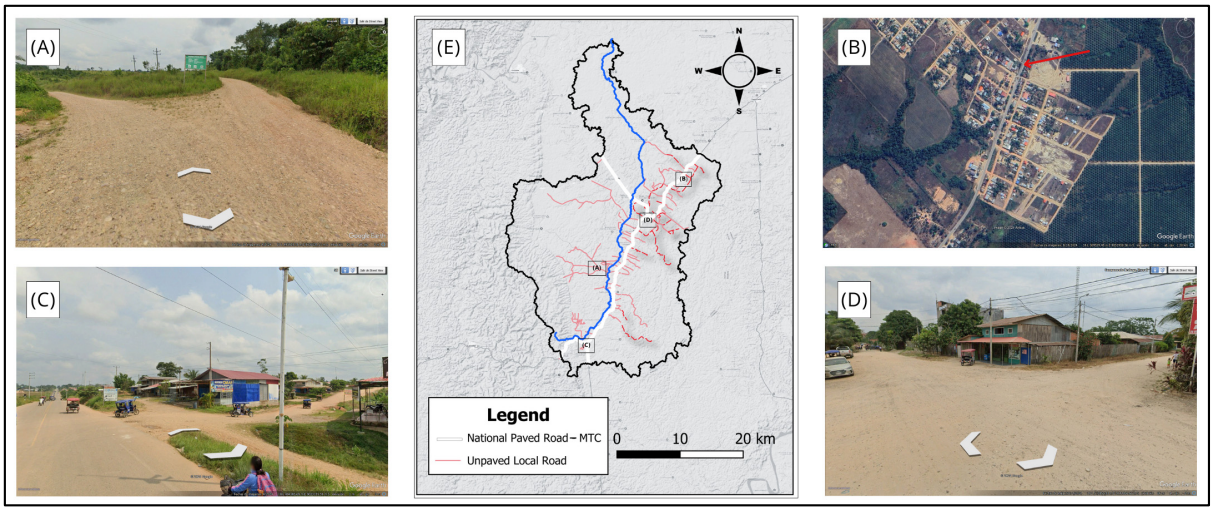

Figure 8. Roads, highways and cities in the Neshuya sub-basin. (**A**) Unpaved roads used for local transport. (**B**) Typical city of the Neshuya sub-basin. Arrow indicates the "Federico Basadre" national highway which is paved. The rest of the roads and highways are not paved. (**C**) Close-up view of the "Federico Basadre" national highway on the left side and unpaved roads on the right side. (**D**) Close-up view of the city, showing unpaved roads. (**E**) Map of the "Federico Basadre" national highway (white lines) and local roads (red line), obtained from the spatial data website of the "Ministry of Transport and Communications of Peru-MTC" (https://portal.mtc.gob.pe/estadisticas/descarga.html) (accessed on 1 November 2024) and prepared in the QGIS software. Images (**A**–**D**) were obtained from Google Earth Pro version 7.3 software.

As a result of the visual interpretation of soil conservation activities, a value of 1 was considered suitable for the whole sub-basin, since no conservation practices were observed. Also, roads were not paved in the majority of the cases during the 2016 and 2022 period.

3.6. Erosion

The average erosion in 2016 was calculated to be 3.87 t ha^{-1} year^{-1} with a standard deviation of 6.47, while in 2022, it was 4.55 t ha^{-1} year^{-1} with a standard deviation of 6.96 (Figure 9). The spatial distribution of each level shows a tendency to "high" and "very high" levels towards the western sector of the sub-basin.

Areas belonging to each erosion level increased in 2022 compared to 2016 (close-ups of Figure 9). It is also observed that areas with "high" and "very high" erosion levels increased more in the west and southwest sectors. On the other hand, areas with erosion levels classified as "very low", decreased from 579.83 km^2 in 2016 to 530.05 km^2 in 2022, while other areas classified with erosion levels from "low" to "very high", increased. This indicates that by 2022, 49.78 km^2 of surface area increased its risk of suffering erosion compared to 2016. The areas of "low" erosion increased by 18.8 km^2; those of "slightly

moderate" erosion, by 9.75 km^2; those with "moderate" erosion, in 6.79 km^2; those with "high" erosion, in 6.94 km ^{2} and those with "very high" erosion, in 7.50 km^2 (Table 9).

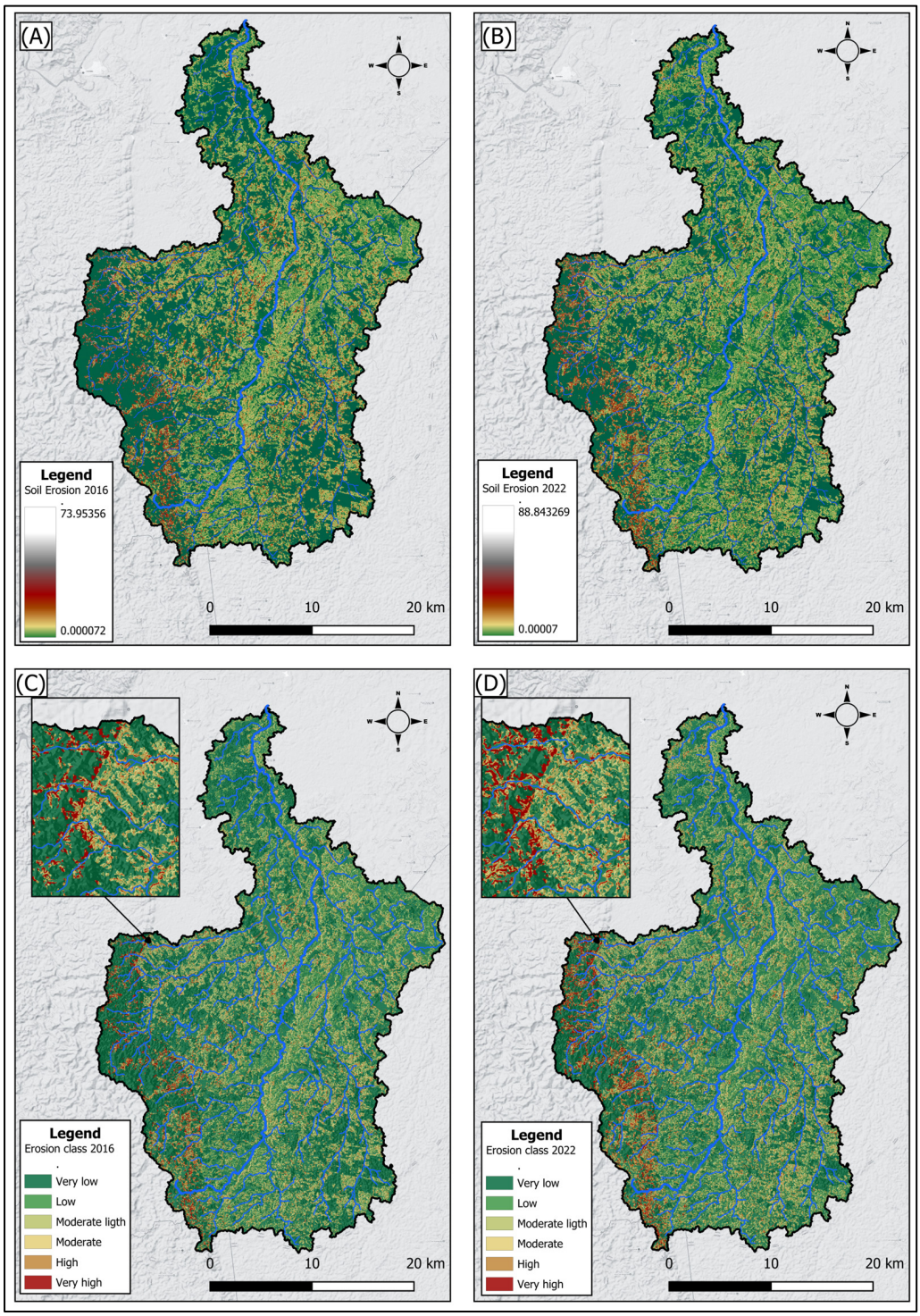

Figure 9. Spatial distribution of the soil erosion in t ha^{-1} year^{-1} in 2016 (**A**) and 2022 (**B**). Estimated erosion in 2016 (**C**) and 2022 (**D**) in the Neshuya River sub-basin based on RUSLE. Average erosion 3.87 t ha^{-1} year^{-1}, standard deviation 6.47 (2016). Average erosion 4.5 t ha^{-1} year^{-1}, standard deviation 7.04 (2022). Images produced with QGIS software (version 3.34.6-Prizren http://www.qgis.org/) [50].

Table 9. Area of erosion levels in 2016 and 2022 and their change.

Erosion Category	Soil Loss in t ha^{-1} Year^{-1}	2016 Area (km^2)	2022 Area (km^2)	Change Areas (km^2)	Rate (%)
Very low	0–2.5	579.83	530.05	−49.78	−5.12%
Low	2.5–5	117.37	136.17	18.80	1.93%
Moderately high	5–10	155.73	165.48	9.75	1.00%
Moderate	10–15	59.96	66.75	6.79	0.70%
High	15–25	43.07	50.01	6.94	0.71%
Very high	25–225	17.02	24.51	7.50	0.77%

The special distribution of erosion (Figure 9A,B) shows that the highest values of erosion are found in the western region of the sub-basin and the values for 2022 exceed those of 2016 by approximately 20%. It is observed that in 2022, the red areas seem to expand, indicating an increase in the severity of erosion compared to 2016; in parallel, the green areas were slightly reduced, indicating that erosion is affecting even the most stable areas.

If we analyze how the erosion levels have varied for each type of vegetation cover (Figure 10, Supplementary Materials—S11), we see that the forest type category that groups both types (non-flooded and flooded forest) shows a notable decrease in the "very low" erosion level. This went from having 345.74 km^2 to 238.24 km^2. That is, 105.5 km^2 increased their erosion levels in a period of 6 years. The "low" and "slightly moderate" erosion levels also showed a reduction, but only 1.3 km^2 (Figure 10). On the other hand, the "high" and "very high" erosion levels showed a slight increase of 0.06 km^2 and 0.12 km^2, respectively. In general, forest area decreased by 107.96 km^2. This indicates that a large part of forested areas with low erosion levels became part of the other types of vegetation cover (Figure 10). The agricultural mosaic showed a slight decrease in the areas with "very low" and "low" erosion levels. In a period of 6 years, they were reduced by 12.79 km^2 and 8.31 km^2, respectively. Areas with "slightly moderate" erosion levels suffered the most dramatic reduction. They went from 117.28 km^2 in 2016 to 38.60 km^2 in 2022 (Figure 10). This indicates a decrease of 78.68 km^2. On the other hand, the areas with "moderate" erosion levels increased from 48.06 km^2 to 106.88 km^2, which is an increase of 58.82 km^2. The areas with "high" and "very high" erosion levels increased by 10.25 km^2 and 5.28 km^2, respectively. These increases in erosion levels may be related to little or no soil conservation practices on farmland. It was also observed that areas of agricultural mosaic decreased by 25.43 km^2 (Figure 10). In oil palm, areas with "very low" erosion went from 58.17 km^2 to 82.50 km^2 during the study period, while areas with "low" levels went from 38.86 km^2 to 56.11 km^2. This may be a consequence of the transformation of forest areas, agricultural mosaic or pastures to oil palm plantations. The areas with "moderately light" erosion decreased by 26.4 km^2. However, areas with "moderate" erosion increased from 9.25 km^2 to 48.17 km^2. Areas with "high" and "very high" erosion increased by 9.76 km^2 and 0.19 km^2, respectively. This could be related to soil management practices that do not prioritize soil conservation (Figure 10). Pastures showed a substantial increase in area with "very low" erosion. They went from 14.45 km^2 to 56.25 km ^{2}. The areas with "low" erosion went from 5.75 km^2 to 14.93 km^2. This could be due to the transformation of low-erosion forested areas into pastures. The other categories remained constant, however, when observing the total increase in pasture area, it can be seen that it went from 23.75 km^2 to 78.90 km^2. This means that in a period of 6 years, 55.15 km^2 of soil was transformed into pastures (Figure 10). Bare soil includes roads, cities and exposed soil (Figure 8). Overall, an increase of 13.17 km^2 was observed during the study period. Areas with "very low"

erosion increased from 1.45 km^2 to 5.18 km^2, while those with "low" erosion increased from 0.4 km^2 to 1.2 km^2. All other categories did not increase by more than 2.5 km^2 (Figure 10). However, it should be noted that bare soils are the most susceptible to erosion.

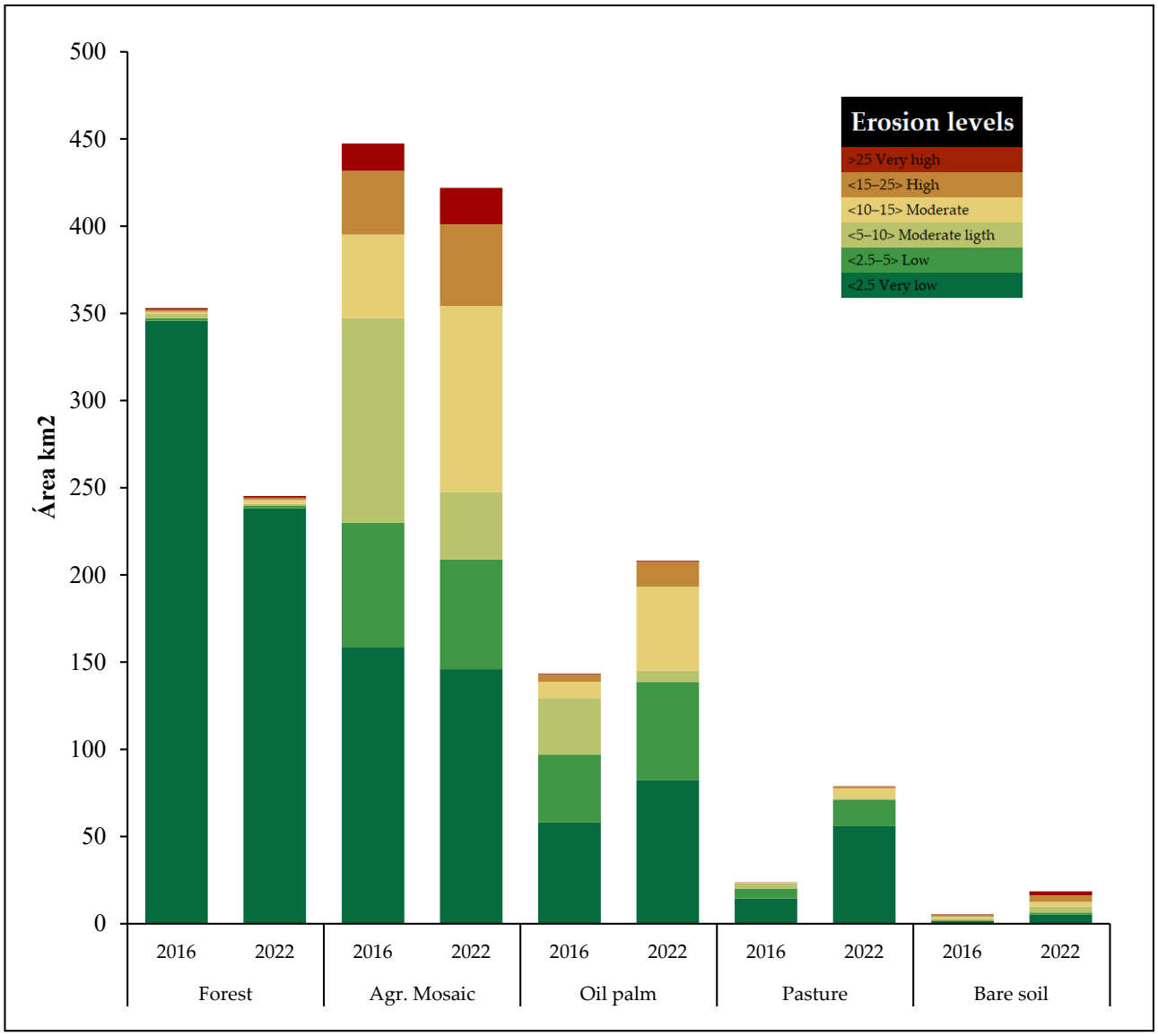

Figure 10. Erosion levels by land cover type. "Forest" category incorporates non-flooded and flooded. "Agr. Mosaic" category considers crops such as cassava, maize, banana, papaya and cocoa. "Bare soil" category includes roads, exposed soil, cities and towns. Additional details can be found in Supplementary Materials—S11.

In total, 74.52 km^2 (7% of the sub-basin) exceeded the soil loss tolerance (SLT) in 2022, while 107.96 km^2 were deforested from 2016 to 2022. The spatial distribution between the deforested areas and erosion zones that exceed the soil loss tolerance ("high" and "very high") shows a clear correlation (Figure 11). The areas with the greatest forest loss are located in the eastern and southeastern areas of the sub-basin. These sectors coincide with the areas with the highest levels of erosion. On the other hand, in the eastern area, the relationship between deforestation and erosion is less evident; deforestation continues to be a determining factor in the increase in erosion. It is also observed that many of the "high" and "very high" erosion zones are located near watercourses (blue lines) (Figure 11).

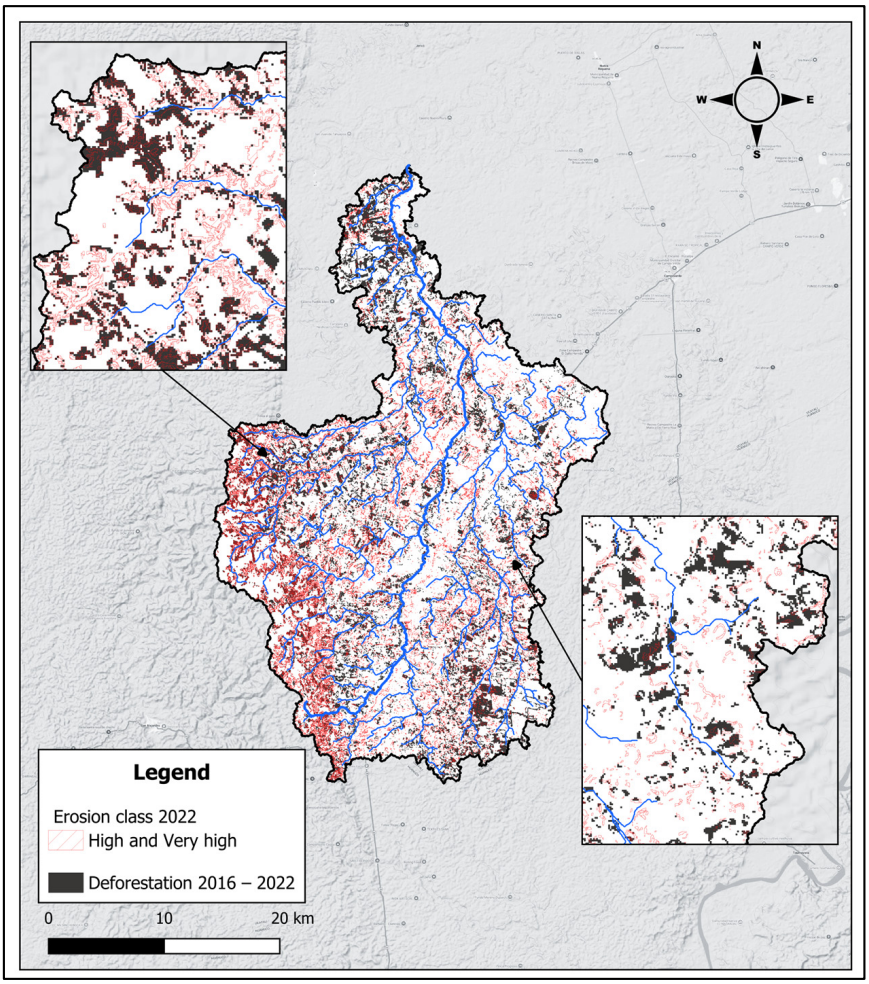

Figure 11. Spatial distribution of forest loss (black polygons) in the period 2016–2022 and location of áreas with 'very high' and 'high' erosion levels (red colored lines). These values are abobe the tolerance threshold of soil loss, in the Neshuya sub-basin, Ucayali region. Images produced with QGIS software (version 3.34.6-Prizren http://www.qgis.org/) [50].

4. Discussion

This study aimed to determine the increase in erosion levels and their spatial distribution due to the decrease in natural forest cover and the increase in agricultural area. We hypothesized that, in the Neshuya sub-basin, water erosion calculated with the RUSLE hydrological model increased considerably in 2022, compared to the 2016 scenario. This was due to the loss of forest cover (ha) and the change in land use oriented towards agricultural activities (ha). It was also suggested that the introduction of various cultivated species caused an alteration in the exposure of the soil to precipitation (mm), which modified the properties of the soil and consequently contributed to the increase in erosion levels (t ha^{-1} $year^{-1}$). The hypothesis was confirmed.

The average erosion in the Neshuya sub-basin increased from 3.87 to 4.55 t ha^{-1} $year^{-1}$. This coincides with the value of 3.9 t ha^{-1} $year^{-1}$ estimated by Aybar et al. [13] in the Ucayali region. Erosion rates in this research coincide with studies carried out at similar conditions to Neshuya. For instance, research carried out in Brazil by Lense et al. [8,12] gave a range of erosion between 1.5 to 62.85 t ha^{-1} $year^{-1}$. However, it is much lower than that reported by Alyson Bueno [10], who concludes that deforestation caused an extreme value of 386 t ha^{-1} $year^{-1}$, in an Amazonian basin in Brazil, with very similar environmental conditions to Neshuya. This discrepancy may be explained by the intensity of precipitation in that area. In Malaysia, Kamaludin et al. [64] reported a range from 0 to 95 t ha^{-1} $year^{-1}$

and Rizeei et al. [63] reported higher average values of 143.35 95 t ha^{-1} year^{-1} for 2010 and 162.24 95 t ha^{-1} year^{-1} for 2016. According to Palliyaguru et al. [82] in Sri Lanka, the average erosion increased from 2.81 to 321 t ha^{-1} year^{-1} from 1989 to 2021. Similarly, in Ethiopia, according to Teshome et al. [83], from 1986 to 2020, the average erosion went from 53.2 to 64 t ha^{-1} year^{-1}. These authors agreed that the highest values are related to aspects of deforestation, steeper slopes, sandy soils, palm plantations and poor conservation practices, as occurs in Neshuya. Also in Malaysia [63,64], palm plantations and agricultural activity are the main reasons behind forest area reduction. The situation is similar in Sri Lanka [82,83], but with the exception that in the study basins there are no palm plantations. But in other cases, such as in Brazil [8,12], the study basins also do not have palm in their cover, but they comply with local conditions similar to Neshuya, as in the studies already mentioned.

Overall, it was observed that in the entire Neshuya sub-basin, areas with very low erosion levels were reduced by 49.78 km^2, and became part of the categories with a higher level of erosion (Table 9). This suggests a progressive deterioration of the soil. Although the change in the average erosion of the entire study zone does not reach the dramatic levels of the work of Alyson Bueno [10] in Brazil or the relatively high levels in Malaysia and Ethiopia [63,83], it is possible to see that there was an increase during the study period. This increase can be explained by the relationship between changes in land use and erosion. Forest areas went from 345.74 km^2 in 2016 to 238.24 km^2 in 2022. This means that, in just 6 years, 105.5 km^2 were transformed either into pastures, oil palm plantations, agricultural mosaic or left as bare soil (Table 8, Figure 6).

Heavy rainfall is one of the main erosive agents in the study area [17]. Although there is a discrepancy in the R factor with the results in Brazil (14,852 MJ mm ha^{-1} h^{-1} year^{-1} [10] and 9000–12,000 MJ mm ha^{-1} h^{-1} year^{-1} [8], compared to those found in our study, 1100–2290 MJ mm ha^{-1} h^{-1} year^{-1} (Figure 3), the explanation lays in rainfall having been slightly lower in Neshuya. Despite this, values of rainfall erosivity (R factor) calculated in Neshuya agree with the values reported by [13,84]. On the other hand, the high level of rain aggressiveness expressed as the Modified Fournier Index (MFI > 160) is consistent with other studies conducted in areas with high precipitation values [27,28,30]. Since our research's precipitation and MFI values are directly related to each other, the R factor is confirmed as the main erosive agent.

Regarding the K factor reported in this study, it ranged from 0.00148 to 0.00236 and it coincides with other authors' findings (Table 5). In addition, according to Palliyaguru et al. [82] a well-structured clay soil with adequate plant protection has low erosion levels. However, Valladares et al. and Zaroni et al. [85,86] indicate that Acrisols are susceptible to erosion on moderately undulating slopes, as it is the case in our study area (Figure 5). Similarly, shallow Cambisols found in steep terrain such as in the western part of the basin (Figure 5) are highly erodible [86].

In Ucayali, especially in the Neshuya sub-basin, financial challenges, lack of education and low awareness of the importance of sustainable practices significantly limit the implementation of soil conservation practices. This situation, aggravated by the remoteness of the area, makes it difficult for local farmers to adopt sustainable measures [87–89]. It is very common for lands to be abandoned after they have lost their fertility [7]. Transporting fertilizers to such remote agricultural areas is not economically viable.

How does land use change begin? Initially, selective logging leads to the opening of dirt roads in forest areas. Later, the forests were cleared to make way for crops and pastures for livestock, which in turn, increase the area of dirt roads [90]. This can be seen in Figure 6. In places where vegetation acts as a natural barrier to the indiscriminate entry of people, these precarious roads facilitate the entry of settlers who practice slash and

burn agriculture [39,91]. According to Reyes and Robiglio [90] in Ucayali, most of the roads are not paved, since most are built without authorization from the local government. Asphalt roads are rarely viable, mainly because their construction entails greater losses of biodiversity and increased deforestation in the Peruvian Amazon [92]. In the study area, it was found that the roads area increased from 4.68 to 6.49 km^2 from 2016 to 2022 (Table 8). In 2024, only 0.435 km^2 were observed to be paved (Figure 8). In addition, the width of the paved road does not exceed 7 m, which is less than the pixel size (12.5 m × 12.5 m) with which the erosion analysis was carried out. In previous years, it is estimated that the paved surface was smaller; therefore, it does not represent an important protection factor in the study area.

Once migratory farmers have settled, they transform forest into agricultural mosaic motivated by obtaining subsistence food and surpluses for sale to the local population. After a quick yield decrease in annual crops, land transitions to pastures for livestock [93–95], or to oil palm [96]. This motivates deforestation to maintain their productivity [97,98]. In our research, we found that the area classified as an agricultural mosaic was reduced from 447.40 km^2 to 421.97 km^2 during the study period. However, pastures increased from 23.75 km^2 to 78.80 km^2 and oil palm is the crop that increased its extension the most, from 143.51 km^2 in 2016 to 208.06 km^2 in 2022 (Table 8). This means that in a period of 6 years, the areas of these two crops increased by 55.05 km^2 and 64.55 km^2, respectively. This is because the ecological conditions favor commercially viable palm yields [99]. On the other hand, in Peru the institutional framework is inadequate to order the expansion of this crop following technical criteria of sustainable development [100,101]. Regarding forest cover, a deforestation rate of 17.99 km^2 $year^{-1}$ was found. This is much higher than that calculated by Marcus et al. [18], who estimated a deforestation rate of 3.56 km^2 $year^{-1}$ from 1987 to 2015.

So, how can we explain that land use change has increased erosion levels? The explanation lies in how effective soil cover is when it comes to decreasing the impact force of raindrops, as well as the drag of particles by runoff [78] based on [43]; Gonzales del Tánago 1991 cited by [13]. Forests, being climax ecosystems, incorporate several layers of protection against the force of rain, which is a consequence of the different canopy heights from vegetation at different strata. Likewise, the layer of leaf litter works as the last protective barrier to reduce the impact of raindrops.

In our research, erosion in forest areas was estimated in 0.510 and 0.687 t ha^{-1} $year^{-1}$ for 2016 and 2022, respectively (Supplementary Materials—S12). It goes along with results from Indonesia, estimated at 0.510 t ha^{-1} $year^{-1}$ at similar conditions [66,68]. In the case of the Neshuya sub-basin, after the transition to agricultural mosaic, the set-up of an annual crop leaves the soil exposed to rainfall. Poor soil management practices related to this type of subsistence farming, such as placing crops on the slope (Image xx1, a), favors erosion. In Brazil, Lense et al. [12] found that agricultural expansion on soils naturally covered by forests changed erosion levels from 0.5 to 1.5 t ha^{-1} $year^{-1}$. In our study, we found how the erosion categories "very high", "high" and "moderate" have increased according to what was explained in previous lines (Figure 10 and Supplementary Materials—S11). Furthermore, the average erosion in agricultural mosaic increased from 6.45 to 7.12 t ha^{-1} $year^{-1}$ from 2016 to 2022 (Supplementary Materials—S11). On the other hand, if this transition occurs towards pastures, the level of erosion is much lower because the root system of grasses favors greater aggregate stability compared to annual and perennial crops. In our study, areas with pastures remained within the "low" and "very low" erosion categories predominantly (Table 9), which corroborates the higher degree of aggregate stability. Erosion increases in pastures are mainly related to overgrazing and grassland burning practices [10,86]. Finally, if the transition happens towards oil palm, our study showed that

the level of erosion also tends to increase (Figure 10 and Supplementary Materials—S12), from 0.038–31.11 t ha^{-1} year^{-1} to 0.045–51.66 t ha^{-1} year^{-1} in 2016 and 2022, respectively (Supplementary Materials—S12). These findings corroborate with Rizeei et al. [63] who reported erosion levels that exceed 50 t ha^{-1} year^{-1} for oil palm crops in Malaysia. These values are extreme for that region. Erosion in oil palm plantations is related to the processes of land leveling, tillage and construction of drainage systems. In addition, high levels of compaction have been observed [102]. On the other hand, the application of herbicides limits the natural growth of native plants, which maintains areas of bare soil [103]. Naharuddin et al. [68] indicate that a cocoa agroforestry system can reduce erosion up to three times less compared to a cocoa monoculture. Ramadhan et al. [68] reported average erosion values for oil palm of 89.12 to 122.94 and bare soil of 249.17 t ha^{-1} year^{-1}, respectively. All of the above supports the idea that, in order to reduce erosion, areas covered by forest should be preserved as much as possible. And areas that have already been transformed for agricultural use should incorporate soil conservation and agroforestry practices to reduce erosion and therefore maintain their fertility levels.

After deforestation due to shifting agriculture, soil's fertility decreases as several physical and chemical properties are degraded such as soil structure and reduction of infiltration which increases runoff. Also, organic matter reduces because of a higher exposure to oxygen, which decreases biological fertility and keeps negatively affecting soil structure [36]. Organic carbon has an important role in the configuration of the K factor values according to the Formula (4) proposed by Sharpley et al. [56]. In this regard, Lima et al. mention that it reduces soil erodibility (K Factor) by improving its properties [35]. This is shown in the spatial relationship map of organic carbon with erodibility (Supplementary Materials—S13).

In this study, most of the samples fell in the range from 1 to 3% of organic carbon, since the soil samples come mainly from agricultural plots. These values agree with those reported by Malaga et al. [39] for the same study area. They found 4.69% of organic carbon (forest) and 2.48% (oil palm). On the other hand, the difference with other tropical ecosystems of similar latitude is interesting, such as in Nueva Guinea, a traditional area of palm plantations. Nelson et al. [104] reported 6.5% organic carbon in forest, 5.5% in palm and 5% in pasture (approximate values), which could indicate more sustainable practices in this region in comparison to Neshuya, whose forests are more susceptible to the loss of organic carbon.

5. Conclusions

1. The study showed an increase in average erosion in the Neshuya sub-basin, from 3.87 t ha^{-1} year^{-1} in 2016 to 4.55 t ha^{-1} year^{-1} in 2022, which represents a change of 17.6% between both years. This increase is directly related to the expansion of agricultural activities quantifies in terms of area. It went from 615.05 km^2 in 2016 to 709.4 km^2 in 2022. This means a replacement of 15.3% of the Amazon forest. The hypothesis that the conversion of forest to agricultural land increases erosion is confirmed.
2. The "moderate", "high" and "very high" erosion categories showed an increase in their affected area between 2016 and 2022, with increases of 6.79 km^2, 6.94 km^2 and 7.50 km^2, respectively. This corresponds to the areas with the highest slope (11–35%) located in the eastern part of the sub-basin, where precipitation has a greater incidence with rainfall erosivity rates in a range from 1500 to 2297 MJ mm ha^{-1} h^{-1} year^{-1}.
3. In the study area, soils had a high resistance to erodibility with very low values for the K factor, due to the predominance of clay loam, loam and sandy clay loam textures.

This is consistent with other studies. In addition, a low percentage of organic carbon was not sufficient to increase the erodibility factor.

4. The tolerated erosion was over the limit in 74.52 km^2. This is spatially related to slash-and-burn deforestation (107.96 km^2) near waterways.
5. The "very low" erosion category showed a reduction of 49.78 km^2 (−5.12%) as a result of less sustainable practices. Less susceptible areas to erosion had lower erosivity ranges between 1100 and 1500 MJ mm ha^{-1} h^{-1} $year^{-1}$ and gentler slopes, from 0 to 11%.

Supplementary Materials: The following supporting information can be downloaded at: https://www.mdpi.com/article/10.3390/geosciences15010015/s1., S1: Observed precipitation data from SENAMHI weather stations; S2: Monthly precipitation data obtained from PISCO (Peruvian Interpolated Data from SENAMHI's Climatological and Hidrological observation); S3: Statistical analysis of correlation between precipitation data from observed stations and PISCO; S4: Physical and chemical parameters evaluated from the reports of the Laboratory of Water, Soil and Foliar (LABSAF) of INIA Experimental Station in Pucallpa EEA Pucallpa; S5: Calculating the K-Factor and subfactors at sampling sites; S6: Calculation of soil parameter semi-variogram; S7: Results of the statistical analysis between the observed stations and PISCO; S8: Precipitation data from the 42 fictitious precipitation stations obtained from PISCO; S9: Calculations of the Modified Fournier Index (IFM) for weather stations; S10: Calculating the R-factor from PISCO monthly precipitation data; S11:Area in km^2 of each erosion level by type of cover; S12: Average erosion for each type of soil cover; S13: Mapas de carbono organico (%) and soil erodibility values (factor K).

Author Contributions: Conceptualization, M.A.-S. and C.R.-L.; methodology, M.A.-S. and C.R.-L.; software, M.A.-S.; validation, M.A.-S. and C.R.-L.; formal analysis, M.A.-S.; investigation, M.A.-S. and D.A.-G.; resources, R.S.-A.; data curation, M.A.-S.; writing—original draft preparation, M.A.-S. and C.P.-C.; writing—review and editing, C.P.-C., C.R.-L., R.M.H.-E., D.A.-G. and R.S.-A.; visualization, M.A.-S.; supervision, C.P.-C., R.M.H.-E. and R.S.-A.; project administration, R.S.-A.; funding acquisition, R.S.-A. All authors have read and agreed to the published version of the manuscript.

Funding: This research was funded by the INIA project "Mejoramiento de los servicios de investigación y transferencia tecnológica en el manejo y recuperación de suelos agrícolas degradados y aguas para riego en la pequeña y mediana agricultura en los departamentos de Lima, Áncash, San Martín, Cajamarca, Lambayeque, Junín, Ayacucho, Arequipa, Puno y Ucayali" CUI 2487112.

Data Availability Statement: All data generated during the study can be found in the Supplementary Materials.

Acknowledgments: We would like to acknowledge the collaborators of the EEA Pucallpa for giving us the necessary help to finish this work.

Conflicts of Interest: The authors declare no conflicts of interest.

References

1. FAO. *El Estado Mundial de La Agricultura y La Alimentación 2020*; Organización de las Naciones Unidas para la Agricultura y la Alimentación: Washington, DC, USA, 2020; ISBN 978-92-5-133644-1. [CrossRef]
2. Weil, R.; Brady, N. *The Nature and Properties of Soils*, 15th ed.; Pearson: Essex, UK, 2017.
3. Cisneros, J.; Cholaky, C.; Cantero, G.; Gonzáles, J.; Reynero, M. *Erosión Hídrica: Principios y Técnicas de Manejo*; Universidad Nacional de Río Cuarto: Río Cuarto, Argentina, 2012; ISBN 9789876880244.
4. Vasquez, A. *Manejo de Cuencas Altoandinas*; Universidad Nacional Agraria La Molina: Lima, Peru, 2000; Volume 1, ISBN 978-612-4147-55-5.
5. Boardman, J.; Favis-Mortlock, D. *Modelling Soil Erosion ByWater*; Springer: Berlin/Heidelberg, Germany, 1998; ISBN 978-3-642-63787-2. [CrossRef]
6. Ramirez, F.A.; Hincapié, E.; Sadeghian, S. Erodabilidad de Los Suelos de La Zona Central Cafetera Del Departamento de Caldas. *Centro Nacional de Investigaciones de Café—Cenicafe* **2009**, *60*, 58–71. Available online: https://biblioteca.cenicafe.org/bitstream/10778/157/1/arc060(01)58-71.pdf (accessed on 5 January 2025).

7. Ei-Swaify, S.; Dangler, E.; Armstrong, C. *Soil Erosion by Water in the Tropics*; University of Hawaii: Honolulu, HI, USA, 1982.
8. Lense, G.H.E.; Parreiras, T.C.; Spalevic, V.; Avanzi, J.C.; Mincato, R.L. Soil Losses in the State of Rondônia, Brazil. *Ciência Rural* **2021**, *51*, e20200460. [CrossRef]
9. Lu, D.; Li, G.; Valladares, G.; Batistella, M. Mapping Soil Erosion Risk in Rondônia, Brazilian Amazonia: Using RUSLE, Remote Sensing and GIS. *Land Degrad. Dev.* **2004**, *15*, 499–512. [CrossRef]
10. Alyson Bueno, F. Estimativa de Erosão Em Área de Desflorestamento Da Amazônia, Bacia Do Baixo Rio Acre. *Rev. Geográfica De América Cent.* **2024**, *2*, 247–262. [CrossRef]
11. Ministerio del Ambiente del Gobierno de Peru. Marco Conceptual Para La Neutralidad En La Degradación de Las Tierras. 2020. Available online: https://cdn.www.gob.pe/uploads/document/file/859308/2020_06_16DipticoNDT72_2.pdf?v=1592417234 (accessed on 5 January 2025).
12. Lense, G.H.E.; Avanzi, J.C.; Parreiras, T.C.; Mincato, R.L. Effects of Deforestation on Water Erosion Rates in the Amazon Region. *Rev. Bras. Cienc. Agrar.* **2020**, *15*, 1–7. [CrossRef]
13. Aybar, C.; Lavado-Casimiro, W.; Huerta, A.; Fernández, C.; Vega, F.; Sabino, E.; Felipe-Obando, O. *Uso Producto Grillado Pisco Precipitación Estudios Investigaciones Sistemas Operacionales Monitoreo Pronóstico Hidrometeorlógico*; Ministerio del Ambiente: Lima, Peru, 2017.
14. Coello Fababa, J.C.; Calle Montes, V. Efecto de la corriente en chorro de bajos niveles en la ocurrencia de precipitación en la selva del Peru. *Ecol. Apl.* **2021**, *20*, 147–159. [CrossRef]
15. Paccini, L.; Espinoza, J.C.; Ronchail, J.; Segura, H. Intra-seasonal Rainfall Variability in the Amazon Basin Related to Large-scale Circulation Patterns: A Focus on Western Amazon–Andes Transition Region. *Int. J. Climatol.* **2018**, *38*, 2386–2399. [CrossRef]
16. Ichikawa, M. Degradation and Loss of Forest Land and Land-use Changes in Sarawak, East Malaysia: A Study of Native Land Use by the Iban. *Ecol. Res.* **2007**, *22*, 403–413. [CrossRef]
17. Flores, B.M.; Montoya, E.; Sakschewski, B.; Nascimento, N.; Staal, A.; Betts, R.A.; Levis, C.; Lapola, D.M.; Esquível-Muelbert, A.; Jakovac, C.; et al. Critical Transitions in the Amazon Forest System. *Nature* **2024**, *626*, 555–564. [CrossRef]
18. Marcus, M.; Gutierrez-Velez, V.H.; Cronkleton, P. *Land Use Change in Four Landscapes in the Peruvian Amazon*; CIFOR: Bogor, Indonesia, 2020. [CrossRef]
19. Del Aguila Feijoo, M.; Walker, T.R. Correspondence to the Editor Re: Artisanal and Small-Scale Gold Mining Impacts in Madre de Dios, Peru: Management and Mitigation Strategies. *Environ. Int.* **2018**, *111*, 133–134. [CrossRef]
20. Alarcón Aguirre, G.; Canahuire Robles, R.R.; Guevara Duarez, F.M.; Rodríguez Achata, L.; Gallegos Chacón, L.E.; Garate-Quispe, J. Dynamics of Forest Loss in the Southeast of the Peruvian Amazon: A Case Study in Madre de Dios. *Ecosistemas* **2021**, *30*, 1–11. [CrossRef]
21. Wischmeier, W.H.; Smith, D.D. *Predicting Rainfall Erosion Losses. A Guide to Conservation Planning*; U. S Department of Agriculture, A.H.N. 537., Ed.; Department of Agriculture, Science and Education Administration: Washington, DC, USA, 1978. Available online: https://www.ars.usda.gov/ARSUserFiles/60600505/RUSLE/AH_537%20Predicting%20Rainfall%20Soil%20Losses.pdf (accessed on 5 January 2025).
22. Renard, K.; Foster, G.; Weesies, D.; Mccool, D.; Yoder, D. *Predicting Soil Erosion by Water A Guide to Conservation Planning with the Revised Universal Soil Loss Equation (RUSLE)*; Agriculture Handbook, 703, Ed.; US Department of Agriculture, Agricultural Research Service: Washington, DC, USA, 1997.
23. Barbosa, W.C.d.S.; Guerra, A.J.T.; Valladares, G.S. Soil Erosion Modeling Using the Revised Universal Soil Loss Equation and a Geographic Information System in a Watershed in the Northeastern Brazilian Cerrado. *Geosciences* **2024**, *14*, 78. [CrossRef]
24. Martins, S.G.; Silva, M.L.N.; Avanzi, J.C.; Curi, N.; Fonseca, S. Cover-Management Factor and Soil and Water Losses from Eucalyptus Cultivation and Atlantic Forest at the Coastal Plain in the Espírito Santo State, Brazil. *Sci. For.* **2010**, *38*, 517–526.
25. Arias, M.P.; Saz, M.; Escolano, S. Estimation of Soil Erosion through the RUSLE Model. Case Study: Upper-Middle Basin of Mira River in Andean-Ecuador. *Investig. Geogr.* **2023**, 207–230. [CrossRef]
26. Phinzi, K.; Ngetar, N.S. The Assessment of Water-Borne Erosion at Catchment Level Using GIS-Based RUSLE and Remote Sensing: A Review. *Int. Soil Water Conserv. Res.* **2019**, *7*, 27–46. [CrossRef]
27. Oliveira, P.T.S.; Wendland, E.; Nearing, M.A. Rainfall Erosivity in Brazil: A Review. *Catena* **2013**, *100*, 139–147. [CrossRef]
28. Ramírez, F.; Hincapié, E.; Sadeghian, S. Erosividad de las lluvias en la zona cafetalera central y occidental del Departamento de Caldas. *Cent. Nac. De Investig. De Café Cenicafé* **2007**, *58*, 40–52.
29. Angulo-Martínez, M.; Beguería, S. Análisis de La Erosividad de La Lluvia: Procesos, Índices y Fronteras de Conocimiento. *Cuaternario Geomorfol.* **2013**, *27*, 53–69.
30. Calero Mosquera, D.; Martinez López, C.; Menjivar Flores, J. C Evaluation of Models to Estimate Rainfall Erosivity in Valle Del Cauca, Colombia. *Acta Agron.* **2021**, *70*, 198–210. [CrossRef]
31. Castelán Vega, R.; López Teloxa, L.C.; Tamariz Flores, J.V.; Linares Fleites, G.; Cruz Montalvo, A. Erosión y Pérdida de Nutrientes En Diferentes Sistemas Agrícolas de Una Microcuenca En La Zona Periurbana de La Ciudad de Puebla, México. *Terra Latinoam.* **2017**, *35*, 229. [CrossRef]

32. Arnoldous, H.M.J. *Approximation of the Rainfall Factor in the USLE in Assessment of Erosion*; Wiley: Chichester, UK, 1980; pp. 127–132.
33. Ozsahin, E.; Duru, U.; Eroglu, I. Land Use and Land Cover Changes (LULCC), a Key to Understand Soil Erosion Intensities in the Maritsa Basin. *Water* **2018**, *10*, 335. [CrossRef]
34. Oliveira, P.T.S.D.; Rodrigues, D.B.B.; Alves Sobrinho, T.; Panachuki, E. Estimativa Do Fator Topográfico Da USLE a Partir de Três Algoritmos. *Ambiente E Agua—Interdiscip. J. Appl. Sci.* **2010**, *5*, 217–225. [CrossRef]
35. Lima, C.G.D.R.; Bacani, V.M.; Montanari, R.; Vick, E.P.; Ferreira, C.C.; Silva, E.R.D.S.D. Indirect methodologies for measuring soil erodibility and characterizing its spatial variability. *Mercator* **2021**, *20*, 2. [CrossRef]
36. Silva, M.L.N.; Curi, N.; Lima, J.; Ferreira, M. Evaluation of Indirect Methods for Determination of Erodibility of Brazilian Latosols (Oxisols). *Pesq. Agropec. Bras* **2000**, *35*, 1207–1220. [CrossRef]
37. Silva, A.M.D.; Silva, M.L.N.; Curi, N.; Avanzi, J.C.; Ferreira, M.M. Erosividade Da Chuva e Erodibilidade de Cambissolo e Latossolo Na Região de Lavras, Sul de Minas Gerais. *Rev. Bras. Cienc. Solo* **2009**, *33*, 1811–1820. [CrossRef]
38. Nunes, J.G.; Campos, M.C.C.; Oliveira, F.P.; Nunes, J.C.; Macedo, J.A.B. Tolerância de Perda de Solo Por Erosão Na Região Sul Do Amazonas / Soil Loss Tolerance in Southern Amazon. *Rev. Ambiência* **2012**, *8*, 859–868. [CrossRef]
39. Málaga, N.; Hergoualc'h, K.; Kapp, G.; Martius, C. Variation in Vegetation and Ecosystem Carbon Stock Due to the Conversion of Disturbed Forest to Oil Palm Plantation in Peruvian Amazonia. *Ecosystems* **2021**, *24*, 351–369. [CrossRef]
40. Valdez Campos, J.; Delgado Monsalve, F.; Rodriguez Vasquez, K.I.; Garrido Pérez, S.; Tangoa Tuesta, E. Características Del Suelo y Su Influencia En El Crecimiento de Plantaciones de *Eucaliptus urograndis* En La Región Ucayali. *Rev. De Innovación Y Transf. Product.* **2022**, *2*, e003. [CrossRef]
41. Oliveira, P.; Nearing, M.; Wendland, E. Orders of Magnitude Increase in Soil Erosion Associated with Land Use Change from Native to Cultivated Vegetation in a Brazilian Savannah Environment. *Earth Surf. Process Landf.* **2015**, *40*, 1524–1532. [CrossRef]
42. Almagro, A.; Thomé, T.C.; Colman, C.B.; Pereira, R.B.; Marcato Junior, J.; Rodrigues, D.B.B.; Oliveira, P.T.S. Improving Cover and Management Factor (C-Factor) Estimation Using Remote Sensing Approaches for Tropical Regions. *Int. Soil Water Conserv. Res.* **2019**, *7*, 325–334. [CrossRef]
43. Fournier, F. *Climat et Érosion—La Relation Entre l'érosion Du Sol Parl'eau et Les Précipitations Atmosphériques*; Presses Universitaires de France: Paris, France, 1960.
44. Armijos, E.; Crave, A.; Vauchel, P.; Fraizy, P.; Santini, W.; Moquet, J.S.; Arevalo, N.; Carranza, J.; Guyot, J.L. Suspended Sediment Dynamics in the Amazon River of Peru. *J. South Am. Earth Sci.* **2013**, *44*, 75–84. [CrossRef]
45. Espinoza, R.; Martinez, J.M.; Armijos, E.; Espinoza, J.C.; Filizola, N.; Dos Santos, A.; Willems, B.; Fraizy, P.; Santini, W.; Vauchel, P. Spatio-Temporal Monitoring of Suspended Sediments in the Solimões River (2000–2014). *Comptes Rendus Géosci.* **2017**, *350*, 4–12. [CrossRef]
46. Mouyen, M.; Longuevergne, L.; Steer, P.; Crave, A.; Lemoine, J.M.; Save, H.; Robin, C. Assessing Modern River Sediment Discharge to the Ocean Using Satellite Gravimetry. *Nat. Commun.* **2018**, *9*, 3384. [CrossRef] [PubMed]
47. Soudre, M.; Ricse, A.; Carbajal, Y.; Kobayashi, S.; Sabogal, C.; Alegre, J. Adaptability of Six Native Forest Tree Species to Degraded Lands in Pucallpa, Peruvian Amazon. In *Rehabilitation of Degraded Tropical Forest Ecosystems: Workshop Proceedings*; Center for International Forestry Research (CIFOR): Bogor, Indonesia, 2001; pp. 123–128, ISBN 979-8764-70-6.
48. Kobayashi, S. Landscape Rehabilitation of Degraded Tropical Forest Ecosystems: Case Study of the CIFOR/Japan Project in Indonesia and Peru. *For. Ecol. Manag.* **2004**, *201*, 13–22. [CrossRef]
49. Poggio, L.; De Sousa, L.M.; Batjes, N.H.; Heuvelink, G.B.M.; Kempen, B.; Ribeiro, E.; Rossiter, D. SoilGrids 2.0: Producing Soil Information for the Globe with Quantified Spatial Uncertainty. *SOIL* **2021**, *7*, 217–240. [CrossRef]
50. QGIS Proyecto. Available online: http://www.qgis.org/ (accessed on 27 October 2024).
51. Conrad, O.; Bechtel, B.; Bock, M.; Dietrich, H.; Fischer, E.; Gerlitz, L.; Wehberg, J.; Wichmann, V.; Böhner, J. System for Automated Geoscientific Analyses (SAGA) v. 2.1.4. *Geosci. Model Dev.* **2015**, *8*, 1991–2007. [CrossRef]
52. Aybar, C.; Fernández, C.; Huerta, A.; Lavado, W.; Vega, F.; Felipe-Obando, O. Construction of a High-Resolution Gridded Rainfall Dataset for Peru from 1981 to the Present Day. *Hydrol. Sci. J.* **2020**, *65*, 770–785. [CrossRef]
53. Roque, Q. Validation of the Precipitation Data (1981–2016) of the PISCO v2.1 Product: Meteorological Station, Elevation, Seasonality of the Year, and Climatic Region in the Tumbes Basin, Peru. *Manglar* **2023**, *20*, 41–50. [CrossRef]
54. Funk, C.; Verdin, A.; Michaelsen, J.; Peterson, P.; Pedreros, D.; Husak, G. A Global Satellite-Assisted Precipitation Climatology. *Earth Syst. Sci. Data* **2015**, *7*, 275–287. [CrossRef]
55. Guo, R.; Liu, Y. Evaluation of Satellite Precipitation Products with Rain Gauge Data at Different Scales: Implications for Hydrological Applications. *Water* **2016**, *8*, 281. [CrossRef]
56. Sharpley, A.N.; Williams, J.R. *EPIC-Erosion/Productivity Impact Calculator 1. Model Documentation*; U.S. Department of Agriculture, A.R.S. 1993, Ed.; United States Department of Agriculture: Washington, DC, USA, 1990; Volume 1. Available online: https://agrilife.org/epicapex/files/2015/05/EpicModelDocumentation.pdf (accessed on 5 January 2025).
57. Ahaneku, I.E.; Ezinna, K.C.; Orji, F.N.; Alaneme, G.U.; Chukwudi, E.E. Spatial Distribution of Soil Erodibility Factors in Erosion-Prone Areas in Umuahia, Southeast, Nigeria. *J. Eng. Res.* 2024, *in press*. [CrossRef]

58. Denton, O.A.; Aduramigba-Modupe, V.O.; Ojo, A.O.; Adeoyolanu, O.D.; Are, K.S.; Adelana, A.O.; Oyedele, A.O.; Adetayo, A.O.; Oke, A.O. Assessment of Spatial Variability and Mapping of Soil Properties for Sustainable Agricultural Production Using Geographic Information System Techniques (GIS). *Cogent Food Agric.* **2017**, *3*, 1279366. [CrossRef]
59. NASA ASF Data Search Vertex: Images of Satelite Alos Palsar. Available online: https://search.asf.alaska.edu/#/ (accessed on 27 October 2024).
60. Hydrologic Engineering Center. *HEC-HMS Software*, version 4.1; Hydrologic Engineering Center: Davis, CA, USA, 2024.
61. Desmet, P.J.; Govers, G. A GIS Procedure for Automatically Calculating the USLE LS Factor on Topographically Complex Landscape Units. *Soil Water Conserv.* **1995**, *51*, 427–433. Available online: https://www.jswconline.org/content/51/5/427 (accessed on 5 January 2025).
62. Proyecto MapBiomas Peru Colección 2.0 de Mapas Anuales de Cobertura y Uso Del Suelo Del Peru. Available online: https://peru.mapbiomas.org/herramientas/ (accessed on 27 January 2024).
63. Rizeei, H.M.; Saharkhiz, M.A.; Pradhan, B.; Ahmad, N. Soil Erosion Prediction Based on Land Cover Dynamics at the Semenyih Watershed in Malaysia Using LTM and USLE Models. *Geocarto Int.* **2016**, *31*, 1158–1177. [CrossRef]
64. Kamaludin, H.; Lihan, T.; Ali Rahman, Z.; Mustapha, M.A.; Idris, W.M.R.; Rahim, S.A. Integration of Remote Sensing, RUSLE and GIS to Model Potential Soil Loss and Sediment Yield (SY). *Hydrol. Earth Syst. Sci. Discuss.* **2013**, *10*, 4567–4596. [CrossRef]
65. Department of Irrigation and Drainage, (DID). *Guideline for Erosion And Sediment Control in Malaysia*; Ministry of Natural Resources and Environment Department of Irrigation and Drainage Malaysia: Putrajaya, Malaysia, 2010; ISBN 9789834186722.
66. Ramadhan, S.; Hermansah; Rusman, B.; Yasin, S. Erosion Hazard Index [EHI] on Different Land Use in Sub-Watershed Kaos, Jambi. In *Proceedings of the IOP Conference Series: Earth and Environmental Science*; IOP Publishing Ltd.: Bristol, UK, 2021; Volume 741. [CrossRef]
67. Naharuddin, N.; Malik, A.; Ahyauddin, A. Soil Loss Estimation for Conservation Planning in the Dolago Watershed Central Sulawesi, Indonesia. *J. Ecol. Eng.* **2021**, *22*, 242–251. [CrossRef]
68. Naharuddin. *Konservasi Tanah Dan Air*; Penerbit Media Sains Indonesia: Cimenyan, Indonesia, 2020; ISBN 78-623-95100-1-5.
69. Guimarães, D.V.; Silva, M.L.N.; Curi, N.; Martins, R.P.; Melo Neto, J.O. Modeling of Soil Losses on a Yellow Argisol under Planted Forest. *Floresta E Ambiente* **2019**, *26*, e20160292. [CrossRef]
70. Instituto Privado de Investigación sobre Cambio Climático. Informe de Estimación de la Erosión Hídrica del Suelo a Partir del Modelo USLE en la Vertiente del Pacífico. Santa Lucía Cotzumalguapa, Guatemala: Instituto Privado de Investigación sobre Cambio Climático. 2023. Available online: https://icc.org.gt/wp-content/uploads/2023/03/191.pdf (accessed on 5 January 2025).
71. Ministerio de Transportes y Comunicaciones. Descarga de Datos Espaciales. Ministerio de Transportes y Comunicaciones. Available online: https://portal.mtc.gob.pe/estadisticas/descarga.html (accessed on 20 December 2023).
72. Subedi, A.; Subedi, M.; Gautam, S.; Dahal, S. Temporal Variation of Soil Erosion of Kali Gandaki River. Bachelor's Thesis, Department of Civil and Geomatics Engineering, Pashchimanchal Campus, Pokhara, Nepal, 2017. [CrossRef]
73. Mannigel, A.R.; de Passos, M.; Moreti, D.; Rosa Medeiros, L. Fator Erodibilidade e Tolerância de Perda Dos Solos Do Estado de São Paulo. *Acta Sci. Agron.* **2008**, *24*, 1335. [CrossRef]
74. Lobo, D.; Gabriels, D.; Ovalles, F.; Santibañez, F.; Moyano, M.C.; Aguilera, R.; Urra, N. *Guía Metodológica Para La Elaboración Del Mapa de Zonas Áridas, Semiáridas y Subhúmedas Secas de América Latina y El Caribe*; Programa Hidrológico Internacional de la UNESCO para América Latina y El Caribe., Ed.; 2006; ISBN 9290890886. Available online: https://unesdoc.unesco.org/ark:/48223/pf0000228113.locale=en (accessed on 5 January 2025).
75. Angulo, R.J. Relações Entre a Erodibilidade e Algumas Propriedades de Solos Brasileiros. Master's Thesis, Universidade Federal do Paraná (UFPR), Curitiba, Brazil, 1978. Available online: https://acervodigital.ufpr.br/handle/1884/27471 (accessed on 5 January 2025).
76. Martins, S.G.; Avanzi, J.C.; Silva, M.L.N.; Curi, N.; Fonseca, S. Erodibilidade Do Solo Nos Tabuleiros Costeiros. *Pesqui. Agropecu. Trop.* **2011**, *41*, 322–327. [CrossRef]
77. Marques, J.J.G.S.M.; Curi, N.; Ferreira, M.M.; Lima, J.M.; Silva, M.L.N. Adequação de Métodos Indiretos Para Estimativa Da Erodibilidade de Solos Com Horizonte B Textural No Brasil. *Ciência Do Solo* **1997**, *21*, 447–456. [CrossRef]
78. Abdu, A.; Laekemariam, F.; Gidago, G.; Kebede, A.; Getaneh, L. Variability Analysis of Soil Properties, Mapping, and Crop Test Responses in Southern Ethiopia. *Heliyon* **2023**, *9*, e14013. [CrossRef]
79. Putra, A.; Triyatno, T.; Syarief, A.; Hermon, D. Penilaian Erosi Berdasarkan Metode USLE Dan Arahan Konservasi Pada DAS Air Dingin Bagian Hulu Kota Padang-Sumatera Barat. *J. Geogr.* **2018**, *10*, 1–13. [CrossRef]
80. Franca Rocha, W.J.S.; Vasconcelos, R.N.; Costa, D.P.; Duverger, S.G.; Lobão, J.S.B.; Souza, D.T.M.; Herrmann, S.M.; Santos, N.A.; Franca Rocha, R.O.; Ferreira-Ferreira, J.; et al. Towards Uncovering Three Decades of LULC in the Brazilian Drylands: Caatinga Biome Dynamics (1985–2019). *Land* **2024**, *13*, 1250. [CrossRef]

81. Franca Rocha, W.J.S.; Vasconcelos, R.N.; Duverger, S.G.; Costa, D.P.; Santos, N.A.; Franca Rocha, R.O.; de Santana, M.M.M.; Alencar, A.A.C.; Arruda, V.L.S.; da Silva, W.V.; et al. Mapping Burned Area in the Caatinga Biome: Employing Deep Learning Techniques. *Fire* **2024**, *7*, 437. [CrossRef]
82. Palliyaguru, C.; Basnayake, V.; Makumbura, R.K.; Gunathilake, M.B.; Muttil, N.; Wimalasiri, E.M.; Rathnayake, U. Evaluation of the Impact of Land Use Changes on Soil Erosion in the Tropical Maha Oya River Basin, Sri Lanka. *Land* **2022**, *12*, 107. [CrossRef]
83. Teshome, D.S.; Moisa, M.B.; Gemeda, D.O.; You, S. Effect of Land Use-Land Cover Change on Soil Erosion and Sediment Yield in Muger Sub-Basin, Upper Blue Nile Basin, Ethiopia. *Land* **2022**, *11*, 2173. [CrossRef]
84. Gutierrez, L.; Huerta, A.; Sabino, E.; Bourrel, L.; Frappart, F.; Lavado-Casimiro, W. Rainfall Erosivity in Peru: A New Gridded Dataset Based on GPM-IMERG and Comprehensive Assessment (2000–2020). *Remote Sens.* **2023**, *15*, 5432. [CrossRef]
85. Valladares, G.S.; Bognola, I.A.; Gouvêa, J.R.F. *Levantamento de Reconhecimento de Solos de Média Intensidade Da Gleba Machadinho, RO*; Brasil. 2003. Available online: https://www.infoteca.cnptia.embrapa.br/infoteca/handle/doc/17128 (accessed on 5 January 2025).
86. Zaroni, M.J.; Santos, H.G. Argissolos. Agência Embrapa de Informação Tecnológica (Embrapa). Available online: https://www.embrapa.br/agencia-de-informacao-tecnologica/tematicas/solos-tropicais/sibcs/chave-do-sibcs/argissolos (accessed on 28 July 2024).
87. Moreno-Seceña, J.C.; Nava-Tablada, M.E.; HErnández-Sánchez, M.I. Actitud de Cafeticultores Sobre El Manejo y Conservación de Suelos Del Sitio Ramsar, Cascadas de Texolo. *Agric. Soc. Y Desarro.* **2015**, *12*, 553. [CrossRef]
88. Zalles, J.I. Turismo Basado En Naturaleza y Conservación Biológica: Decisiones de Uso de Suelo En Mindo/ Nature-Based Tourism and Biological Conservation: Land-Use Decisions in Mindo. *Let. Verdes. Rev. Latinoam. De Estud. Socioambientales* **2018**, 178–198. [CrossRef]
89. Collado, L.A.; Alegre, J. Farming Systems on Alluvial Soils and Their Impact on the Economy of the Shipibo-Konibo in Ucayali. *Manglar* **2020**, *17*, 193–201. [CrossRef]
90. Reyes, M.; Robiglio, V. *¿Cómo Es La Deforestación Asociada a Las Carreteras En La Amazonía Peruana? Análisis y Recomendaciones En Tres Estudios de Caso Para Reducir Su Impacto*; Center for International Forestry Research (CIFOR): Bogor, Indonesia, 2023. Available online: https://www.cifor-icraf.org/knowledge/publication/9062/ (accessed on 5 January 2025).
91. Ichikawa, M.; Ricse, A.; Ugarte, J.; Kobayashi, S. Migration Patterns and Land Use by Immigrants under a Changing Frontier Society in the Peruvian Amazon. *Tropics* **2014**, *23*, 73–82. [CrossRef]
92. Larrea-Gallegos, G.; Vázquez-Rowe, I.; Gallice, G. Life Cycle Assessment of the Construction of an Unpaved Road in an Undisturbed Tropical Rainforest Area in the Vicinity of Manu National Park, Peru. *Int. J. Life Cycle Assess.* **2017**, *22*, 1109–1124. [CrossRef]
93. Andrieu, N.; Blundo-Canto, G.; Cruz-Garcia, G.S. Trade-Offs between Food Security and Forest Exploitation by Mestizo Households in Ucayali, Peruvian Amazon. *Agric. Syst.* **2019**, *173*, 64–77. [CrossRef]
94. Blundo-Canto, G.; Cruz-Garcia, G.S.; Talsma, E.F.; Francesconi, W.; Labarta, R.; Sanchez-Choy, J.; Perez-Marulanda, L.; Paz-Garcia, P.; Quintero, M. Changes in Food Access by Mestizo Communities Associated with Deforestation and Agrobiodiversity Loss in Ucayali, Peruvian Amazon. *Food Secur.* **2020**, *12*, 637–658. [CrossRef]
95. Porro, R.; Lopez-Feldman, A.W.; Vela-Alvarado, J.; QuiÑonez-Ruíz, L.P.; Seijas-Cardenas, Z.; Vásquez-Macedo, M.; Salazar-Arista, C.I.; NúÑez-Paredes, V.; Cardenas-Ruiz, J. Forest Use and Agriculture in Ucayali, Peruvian Amazon: Interactions Among Livelihood Strategies, Income and Environmental Outcomes. *Tropics* **2014**, *23*, 47–62. [CrossRef]
96. Bennett, A.; Ravikumar, A.; McDermott, C.; Malhi, Y. Smallholder Oil Palm Production in the Peruvian Amazon: Rethinking the Promise of Associations and Partnerships for Economically Sustainable Livelihoods. *Front. For. Glob. Chang.* **2019**, *2*, 14. [CrossRef]
97. Fearnside, P.M. An Ecological Analysis of Predominant Land Uses in the Brazilian Amazon. *Environmentalist* **1988**, *8*, 281–300. [CrossRef]
98. Luizão, F.J.; Fearnside, P.M.; Cerri, C.E.P.; Lehmann, J. The Maintenance of Soil Fertility in Amazonian Managed Systems. In *Amazonia and Global Change*; Wiley Blackwell: Hoboken, NJ, USA, 2009; pp. 311–336. [CrossRef]
99. Glave, M.; Vergara, K. *¿Agroindustria En La Amazonía?: Posibilidades Para El Desarrollo Inclusivo y Sostenible de La Palma Aceitera En El Peru*; 2016; ISBN 978-9972-615-94-8. Available online: https://repositorio.grade.org.pe/bitstream/handle/20.500.12820/306/boletin33.pdf?sequence=1&isAllowed=y (accessed on 5 January 2025).
100. Dammert, J.L. Promoción y Regulación Ambiental de La Palma Aceitera En El Peru: Aspectos Legales e Institucionales. 2016. Available online: https://repositorio.grade.org.pe/handle/20.500.12820/183 (accessed on 5 January 2025).
101. Dammert J., L. Desafíos y Recomendaciones Ante La Expansión de La Palma Aceitera En La Amazonía Andina; 2014. Available online: https://pdf.usaid.gov/pdf_docs/PA00KK1B.pdf (accessed on 5 January 2025).
102. Adiprasetyo, T.; Purnomo, B.; Handajaningsih, M.; Hidayat, H. The Usage of BIOM3G-Biofertilizer to Improve and Support Sustainability of Land System of Independent Oil Palm Smallholders. *Int. J. Adv. Sci. Eng. Inf. Technol.* **2014**, *4*, 345. [CrossRef]

103. Cabrera, M.; Capparelli, M.V.; Ñacato-Ch, C.; Moulatlet, G.M.; López-Heras, I.; Díaz González, M.; Alvear-S, D.; Rico, A. Effects of Intensive Agriculture and Urbanization on Water Quality and Pesticide Risks in Freshwater Ecosystems of the Ecuadorian Amazon. *Chemosphere* **2023**, *337*, 139286. [CrossRef]
104. Nelson, P.N.; Banabas, M.; Nake, S.; Goodrick, I.; Webb, M.J.; Gabriel, E. Soil Fertility Changes Following Conversion of Grassland to Oil Palm. *Soil Res.* **2014**, *52*, 698. [CrossRef]